JOURNAL OF PETROLOGY | VOLUME 47 | NUMBER 11 | PAGES 2233–2256 | 2006 | doi:10.1093/petrology/egl042

Mineral Chemistry of Peridotites from Paleozoic, Mesozoic and Cenozoic Lithosphere: Constraints on Mantle Evolution beneath Eastern China

JIANPING ZHENG[1,2,3]*, WILLIAM L. GRIFFIN[2], SUZANNE Y. O'REILLY[2], JINSUI YANG[4], TIANFU LI[4], MING ZHANG[2], RUTH Y. ZHANG[5] AND JOHN G. LIOU[5]

[1]STATE KEY LABORATORY OF GEOLOGICAL PROCESSES AND MINERAL RESOURCES, FACULTY OF EARTH SCIENCES, CHINA UNIVERSITY OF GEOSCIENCES, WUHAN 430074, P.R. CHINA

[2]GEMOC ARC NATIONAL KEY CENTRE, DEPARTMENT OF EARTH AND PLANETARY SCIENCES, MACQUARIE UNIVERSITY, NSW 2109, AUSTRALIA

[3]KEY LABORATORY OF ISOTOPE GEOCHRONOLOGY AND GEOCHEMISTRY, GUANGZHOU INSTITUTE OF GEOCHEMISTRY, CHINESE ACADEMY OF SCIENCES, GUANGZHOU 510640, P.R. CHINA

[4]INSTITUTE OF GEOLOGY, CHINESE ACADEMY OF GEOLOGICAL SCIENCES, BAIWANZHUANG ROAD 26, BEIJING 100037, P.R. CHINA

[5]DEPARTMENT OF GEOLOGICAL AND ENVIRONMENTAL SCIENCES, STANFORD UNIVERSITY, CA 94305, USA

Downloaded from http://petrology.oxfordjournals.org/ at University of New Orleans on June 26, 2014

RECEIVED NOVEMBER 4, 2005; ACCEPTED AUGUST 1, 2006; ADVANCE ACCESS PUBLICATION AUGUST 22, 2006

Major- and trace-element data on the constituent minerals of garnet peridotite xenoliths hosted in early Paleozoic (457–500 Ma) kimberlites and Neogene (16–18 Ma) volcanic rocks within the North China Craton are compared with those from the pre-pilot hole of the Chinese Continental Scientific Drilling Project (CCSD-PP1) in the tectonically exhumed Triassic (∼220 Ma) Sulu ultrahigh-pressure (UHP) terrane along its southern margin. P–T estimates for the Paleozoic and Neogene peridotite xenoliths reflect different model geotherms corresponding to surface heat flows of $\sim 40\,mW/m^2$ *(Paleozoic) and* $\sim 80\,mW/m^2$ *(Neogene). Garnet peridotite xenoliths or xenocrysts from the Paleozoic kimberlites are strongly depleted, similar to peridotites from other areas of cratonic mantle, with magnesium olivine (mean* $Fo_{92\cdot 7}$*), Cr-rich garnet and clinopyroxene with high La/Yb. Garnet (and spinel) peridotite xenoliths hosted in Neogene basalts are derived from fertile mantle; they have high* Al_2O_3 *and* TiO_2 *contents, low-Mg-number olivine (mean* $Fo_{89\cdot 5}$*), low-Cr garnet and diopside with flat rare earth element (REE) patterns. The differences between the Paleozoic and Neogene xenoliths suggest that a buoyant refractory lithospheric keel present beneath the eastern North China Craton in Paleozoic times was at least partly replaced by younger, hotter and more fertile lithospheric mantle during Mesozoic–Cenozoic times. Garnet peridotites from the Sulu UHP terrane have less magnesian olivine (*$Fo_{91\cdot 5}$*), and lower-Cr garnet than the Paleozoic xenoliths. The diopsides have low heavy REE (HREE) contents and sinusoidal to light REE (LREE)-enriched REE patterns. These features, and their high Mg/Si and low CaO and* Al_2O_3 *contents, indicate that the CCSD-PP1 peridotites represent a moderately refractory mantle protolith. Details of mineral chemistry indicate that this protolith experienced complex metasomatism by asthenosphere-derived melts or fluids in Mesoproterozoic, and subsolidus re-equilibration involving fluids/melts derived from the subducted Yangtze continental crust during UHP metamorphism in the early Mesozoic. Tectonic extension of the subcontinental lithospheric mantle of the North China Craton and exhumation of the Sulu UHP rocks in the early Mesozoic induced upwelling of the asthenosphere. Peridotites sampled by the Neogene basalts represent newly formed lithosphere derived by cooling of the upwelling asthenospheric mantle in Jurassic–Cretaceous and Paleogene time.*

*Corresponding author. Fax: +86 27 6788 3873. E-mail: jpzheng@cug.edu.cn and jpzheng2003@yahoo.com

© The Author 2006. Published by Oxford University Press. All rights reserved. For Permissions, please e-mail: journals.permissions@oxfordjournals.org

KEY WORDS: *garnet peridotite xenoliths; North China Craton; lithospheric thinning; Sulu UHP terrane; UHP lithosphere evolution; mantle replacement*

INTRODUCTION

Apart from remotely sensed geophysical datasets, petrological information on the lithospheric mantle can be obtained from two main sources—tectonically exhumed massifs, including ultrahigh-pressure (UHP) peridotite terranes, and peridotite xenoliths in volcanic rocks (basalts and kimberlites). Eastern China is an important region for the study of lithospheric mantle evolution, in part because of the occurrence of Paleozoic diamondiferous kimberlites (Chi *et al.*, 1996) and Cenozoic basalts, both of which exhume deep-seated mantle xenoliths (Fan & Hooper, 1989). This region also contains the world's largest UHP metamorphic belt in the Triassic Dabie–Sulu terrane, which contains abundant coesite-bearing (Okay *et al.*, 1989; Wang *et al.*, 1989) and diamond-bearing (Xu *et al.*, 1992) eclogites and garnet peridotites (Yang & Jahn, 2000; Zhang *et al.*, 2000, 2003).

Studies of peridotite xenoliths brought to the surface by Paleozoic kimberlites and Cenozoic basalts in the North China Craton (NCC) offer a unique glimpse into the properties and evolution of the Phanerozoic lithospheric mantle. Garnet peridotite xenoliths (Zheng & Lu, 1999) and xenocrysts (Zhou *et al.*, 1994; Griffin *et al.*, 1998*a*) in kimberlites document the presence of a thick lithospheric root at least as late as middle Ordovician times beneath at least part of the NCC. However, Cenozoic basalt-hosted xenoliths are mainly spinel peridotites (Zheng, 1999; Chen *et al.*, 2001) and most have been derived from a thin, hot and fertile lithosphere (Zheng, 1999; Xu *et al.*, 2000; Gao *et al.*, 2002); volcanic rocks in some areas in the interior of the NCC, such as near Hebi, appear to sample shallow relics of the older cratonic mantle (Zheng *et al.*, 2001). The difference suggests the partial replacement of ancient lithospheric mantle by younger material (Griffin *et al.*, 1992, 1998*a*; Menzies *et al.*, 1993; Xu *et al.*, 1998; Zheng *et al.*, 1998). Knowledge of the Mesozoic lithospheric mantle, therefore, can enhance our understanding of the lithospheric evolution in the region (Menzies & Xu, 1998; Fan *et al.*, 2001; Xu, 2001).

The Dabie–Sulu orogenic belt along the south margin of the NCC (Fig. 1) resulted from the early Mesozoic collision between the North China and Yangtze (YC) Cratons (~220 Ma, Li *et al.*, 1993; Jahn, 1998). Abundant occurrences of garnet peridotite, pyroxenite and eclogite in the Sulu area have been extensively investigated in terms of petrology, geochemistry and geochronology. The occurrence of micro-diamonds (Xu *et al.*, 1992) and coesite (Okay *et al.*, 1989; Wang *et al.*, 1989; Hirajima *et al.*, 1990) in the UHP rocks, *P–T* estimates and studies of microstructures in the garnet peridotites (Yang *et al.*, 1993; Zhang *et al.*, 2000, 2003) imply deep subduction of continental lithosphere (Liou *et al.*, 2000; Ye *et al.*, 2000). Garnet peridotites from the Sulu terrane have been considered to be derived from different volumes of a heterogeneous mantle lithosphere, which had experienced complex metasomatic episodes and subsequent UHP metamorphism during the Triassic collision of the North China and Yangtze Cratons (Zheng *et al.*, 2005*a*).

Fig. 1. Localities of Paleozoic–Cenozoic peridotite xenoliths in the North China Craton and the Sulu UHP terrane along the southern margin of the Craton. Mengyin and Fuxian, Paleozoic (457–500 Ma) kimberlite; Fuxin, late Mesozoic (100 Ma) basalt; Cenozoic basalts: Hannuoba, 22 Ma; Shanwang, 16 Ma; Qixia, 12 Ma; Hebi, 4 Ma; Nushan, <2 Ma. NCC, North China Craton; YC, Yangtze Craton; Dabie–Sulu, UHP Belt; CCSD-PP1, the pre-pilot hole of the Chinese Continental Scientific Drilling Project.

A comparative study of the Paleozoic and Cenozoic peridotite xenoliths and peridotites from the UHP terrane has been undertaken. We present data on the major and trace element compositions of minerals in mantle-derived garnet peridotites from the pre-pilot hole of the Chinese Continental Scientific Drilling Project (CCSD-PP1), xenoliths and xenocrysts from the Paleozoic Mengyin kimberlites, and xenoliths from the Cenozoic Shanwang basalts (Fig. 1). These data provide constraints on the composition and mineralogy of the subcontinental lithospheric mantle (SCLM) in eastern China in three time slices. Published data on the Mesozoic (e.g. Xinyang and Fuxin) and Cenozoic (e.g. Hannuoba, Qixia, Hebi and Nushan) spinel peridotite xenoliths from other localities within the North China Craton (Fig. 1) are also considered.

Mantle xenoliths from the early Mesozoic (206–178 Ma; Lu *et al.*, 2003) Xinyang volcanoclastic diatremes in the southwestern part of the North China Craton are refractory spinel-facies peridotite

Downloaded from http://petrology.oxfordjournals.org/ at University of New Orleans on June 26, 2014

(Zheng *et al.*, 2005*b*). The Fuxin and Hannuoba basalts in the eastern and western parts of the northern margin of the craton erupted in late Mesozoic (100 Ma) and Miocene (22 Ma) time, respectively; their xenoliths are dominantly fertile lherzolites with some more refractory xenoliths (Chen *et al.*, 2001; Rudnick *et al.*, 2004; Yu *et al.*, 2006; Zheng *et al.*, 2006*a*). The Qixia and Hebi basalts lie east and west of the Tanlu fault zone and erupted at 12 Ma and 4 Ma, respectively. The Qixia samples are mainly fertile lherzolite (Zheng *et al.*, 1998) with Phanerozoic ages (Gao *et al.*, 2002). The peridotitic xenoliths from Hebi, relatively distant from the Tanlu fault zone, are mainly refractory harzburgite and Cpx-poor lherzolite, and have been interpreted as shallow relics of the Archean cratonic mantle (Zheng *et al.*, 2001). The Cenozoic Nushan basalts, within the Tanlu fault zone in the southeastern part of the craton, erupted at < 2 Ma (Xu *et al.*, 1998).

In this study we compare garnet peridotites from three tectonic settings in and around the North China Craton. We use these data, and previously published data on garnet- and spinel peridotites from other localities in the area, to discuss the evolution of the Sulu UHP peridotites and their relationship to the complex evolution of the lithospheric mantle beneath the North China Craton.

GEOLOGICAL SETTING

The NCC has a Precambrian basement consisting mainly of gneiss, migmatite, and high-pressure granulite-facies rocks (Zhao *et al.*, 1999, 2000; Zhai *et al.*, 2001). The oldest upper-crustal component has an age of 3·8 Ga (Liu *et al.*, 1992); lower-crustal xenoliths from the southern margin of the NCC indicate protoliths of at least this age (Hf model ages of Archean zircon; Zheng *et al.*, 2004*a*). A series of tectonic events occurred in the late Archean and Proterozoic (Jahn, 1990; He *et al.*, 1992), with stabilization in the late Proterozoic (Ernst, 1988); this was followed by a period of magmatic and tectonic quiescence until the eruption of Paleozoic (middle Ordovician) kimberlites.

Diamondiferous kimberlites erupted through late Archean to Ordovician country rocks in Mengyin and Fuxian Counties (Fig. 1). There are abundant peridotite (Zheng & Lu, 1999) and granulite (Zheng *et al.*, 2004*b*) xenoliths in both the Mengyin and Fuxian kimberlites. All of the Paleozoic xenoliths or xenocrysts reported in this paper were collected from Shengli No. 1, the largest of more than 20 pipes in the Mengyin field (Shandong Province). The pipe has an elliptical outline measuring *c.* 230 m × 150 m, and is composed of diatreme-facies macrocrystal porphyritic kimberlite and subordinate hypabyssal facies kimberlite. Rb–Sr and Sm–Nd dating has yielded ages of 457–500 Ma for the kimberlite (Lu *et al.*, 1998).

The Neogene Shanwang basalts, 200 km NE of the Paleozoic Mengyin kimberlite (Fig. 1), include alkali olivine basalt, olivine nephelinite, and basanite; there are three episodes of volcanism. Abundant lherzolite xenoliths (Zheng *et al.*, 1998), including the garnet-bearing peridotites reported in this paper, were collected from the lavas of episode one, which have an eruption age of 18·2–16·8 Ma (whole-rock K–Ar method; Jin, 1985). The Sr–Nd isotopic compositions of the host basalts (Zhi *et al.*, 1994) and spinel peridotite xenoliths (Zheng, 1999; Fan *et al.*, 2001) indicate that they were derived from a depleted mantle source.

Structural, petrological and geochronological data for the Dabie–Sulu orogenic belt indicate that the subduction of the margin of the Yangtze Craton commenced in the late Permian or early Triassic. This was followed by Triassic continental collision and late Jurassic to early Cretaceous exhumation (Li *et al.*, 1993). Many lines of evidence indicate that the UHP terrane consists of Proterozoic supracrustal rocks together with mafic–ultramafic rocks, which all experienced the Triassic UHP metamorphism (Liou *et al.*, 1996; Carswell *et al.*, 2000; Hirajima & Nakamura, 2003). The pre-pilot hole of the Chinese Continental Scientific Drilling Project (CCSD-PP1, Fig. 1), located at the reservoir near the village of Zhimafang, about 9 km south of Donghai City, was drilled to a depth of 432 m with more than 80% core recovery. The lithological profile of the hole includes 47·7% paragneiss (at 41–138, 256–299, 317–337 and 360–432 m), 27·3% peridotites (at 138–256 m except 3 m paragneiss at 238–241 m), 19% orthogneiss, 2·7% eclogite (at 127–130 and 421–425 m), and minor kyanite quartzite and epidote–biotite schist. The peridotitic body is in fault contact with the paragneiss. The gneiss consists of two feldspars + quartz + epidote + phengite + biotite, and contains zircon grains with coesite inclusions (Liu *et al.*, 2001).

SAMPLE DESCRIPTIONS

The Mengyin xenoliths have wide range in microstructure from porphyroclastic through sheared to fine-grained. My0211 and My0278 are the only peridotite samples in our collections that contain fresh garnet, olivine, enstatite and diopside. They are ellipsoidal in shape and show porphyroclastic texture. Coarse-grained garnet, up to 12 mm in diameter, is set in a matrix that consists mainly of serpentine and minor calcite and talc. A few relics of olivine, orthopyroxene and clinopyroxene are found in the matrix. The coarse-grained garnets have a thin (0·1–2 mm) kelyphitic rim, and contain inclusions of diopside and serpentinized olivine (Fig. 2a) or dolomite (e.g. My0278). Heavy-mineral concentrates consisting mainly of garnet with minor olivine and diopside were collected from the Shengli No. 1 kimberlite.

Downloaded from http://petrology.oxfordjournals.org/ at University of New Orleans on June 26, 2014

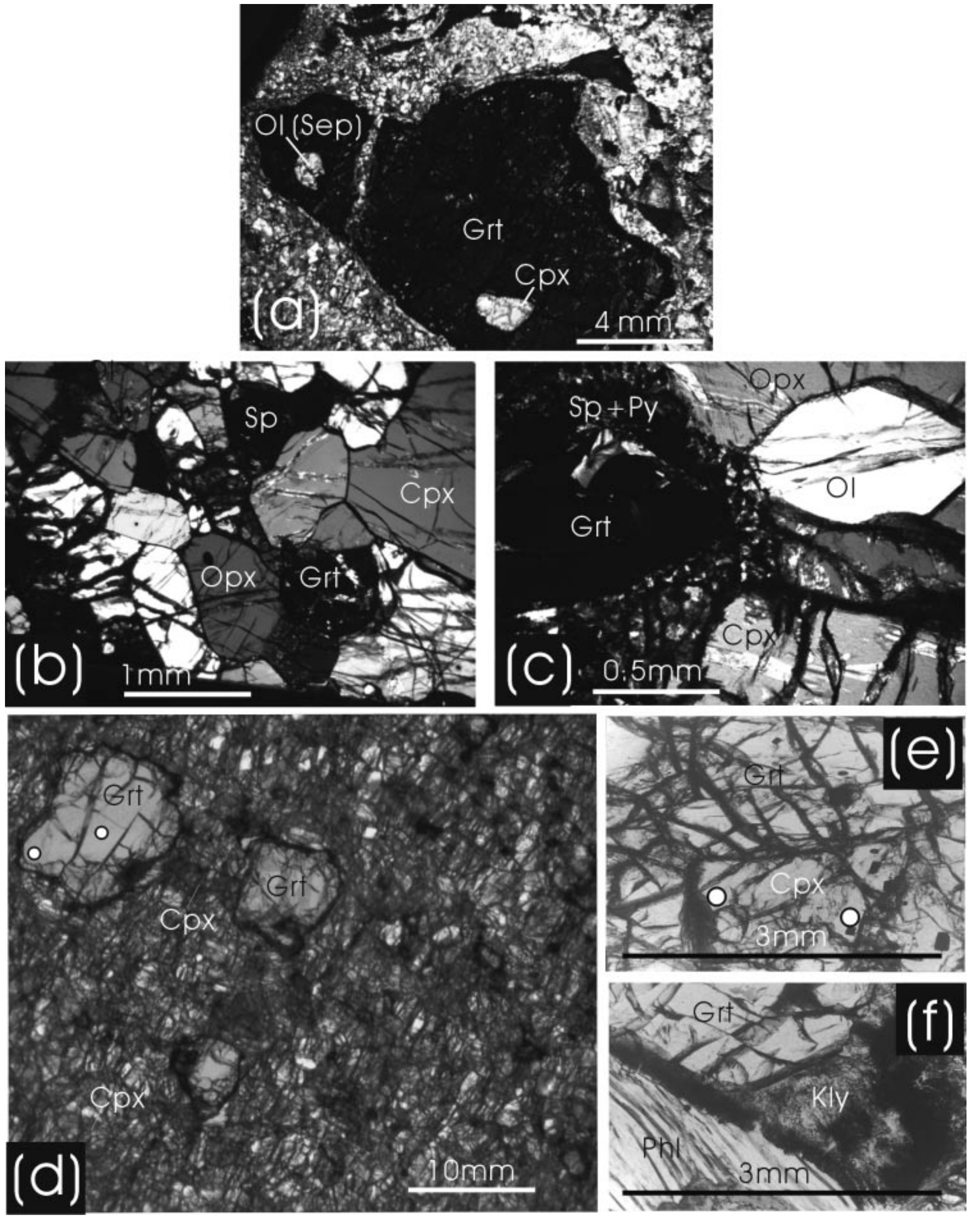

Fig. 2. Photomicrographs of peridotitic xenoliths from eastern China. (a) Garnet with inclusions of olivine (serpentinized) and clinopyroxene in Paleozoic peridotitic xenolith from Mengyin (sample MY0211). (b) and (c) peridotitic xenoliths from Shanwang basalts: (b) garnet coexisting with spinel without reaction rim in spinel–garnet lherzolite with sheared to fine-grained microstructure (SW0193); (c) garnet with reaction rim of fine-grained spinel and pyroxenes in garnet lherzolite (SW01-8). (d)–(f) garnet lherzolite (ZMF7) from Donghai UHP terrane: (d) porphyroblastic garnet set in a matrix of olivine, enstatite, garnet (Grt) and clinopyroxene (Cpx); (e) granular garnet and clinopyroxene in the matrix; (f) phlogopite coexisting with the kelyphitic rim of garnet (Kly). Circles in (d) and (e) show the positions of LAM–ICPMS analyses for garnet and clinopyroxene (Table 7).

These xenocrysts have similar compositions to the minerals in the peridotite xenoliths, and anhedral shapes; they therefore are interpreted as debris from disaggregated xenoliths.

The peridotite xenoliths from Shanwang (5–6 cm in diameter) are mainly fine-grained, foliated, Cpx-rich spinel lherzolites (8·2–19·5 modal % Cpx) with minor Cpx-poor varieties. The garnet-bearing peridotites studied here have porphyroclastic (SW0169 and SW0193), sheared (SW01-1 and SW01-8) and fine-grained (SW04-2 and SW04-6) microstructures as defined by Harte (1977). Garnet coexists with spinel without reaction rims (Fig. 2b) in most of the samples (e.g. SW0169, SW0193, SW04-2 and SW04-6), suggesting that they were derived from the garnet–spinel transition zone. However, in some peridotites garnets

Downloaded from http://petrology.oxfordjournals.org/ at University of New Orleans on June 26, 2014

show reaction rims consisting mainly of fine-grained spinel and pyroxenes (e.g. SW01-1 and SW01-8; Fig. 2c). The modal mineralogy of the peridotites was determined by point counting (Table 1) and the rocks were classified using the IUGS scheme (Le Maitre, 1982).

The CCSD-PP1 peridotites include major garnet lherzolite and harzburgite (ZMF2 and ZMF11) and minor wehrlite and dunite with porphyroblastic (ZMF6, ZMF7 and ZMF8) and sheared (ZMF2, ZMF3, ZMF4 and ZMF11) microstructures (Table 2). They are composed of garnet, olivine, enstatite and diopside (0–7 vol. %), together with minor foliated phlogopite and rare secondary amphibole (ZMF3, ZMF4 and ZMF7). Porphyroblastic garnets (5–15 mm in size, Fig. 2d) are set in a matrix of medium-grained (2–3 mm) olivine seamed by serpentine, with granular pyroxene (enstatite and diopside) and garnet. Some large garnet grains have composite olivine–enstatite–spinel inclusions (e.g. ZMF7). Most garnets have a thin (0·05 mm) kelyphitic rim consisting of radial aggregates of enstatite and diopside (Fig. 2e). Phlogopite grows along micro-cracks or on the kelyphitic rims of garnet (Fig. 2f). Sample ZML, an old drill-core sample from near the CCSD-PP1, was supplied by the Donghai geological team. It has similar petrography to ZMF6 and ZMF7; a detailed description has been given by Zheng *et al.* (2005*a*).

ANALYTICAL METHODS

Major element analyses of minerals (Tables 1–4) were carried out in the GEMOC National Key Centre at Macquarie University using a Cameca SX50 electron microprobe (EMP), fitted with five crystal spectrometers, using an accelerating voltage of 15 kV and a sample current of 20 nA. The width of the electron beam was 5 μm. Standards were natural minerals, and matrix corrections were made after the method of Pouchou & Pichoir (1984). Counting times were 10 s for peaks and 5 s for background on either side of the peak. To examine whether equilibrium had been attained, considerable attention was paid to determining the homogeneity of individual phases. The minerals in the peridotitic xenoliths are homogeneous within analytical precision. In most of the Sulu UHP peridotites, minerals such as garnet and clinopyroxene (e.g. ZMF3, ZMF6, ZMF7 and ZMF8) show some heterogeneity between core and rim (Table 2).

Trace-element analyses of minerals (Tables 3–7) also were carried out at Macquarie University, using a 266 nm UV laser ablation microprobe coupled to an inductively coupled plasma mass spectrometry (LAM–ICPMS) system. The laser ablation system is similar to the one described by Xu *et al.* (2000). The laser is a Continuum Surelite I-20 Q-switched and frequency quadrupled Nd:YAG laser with a fundamental infrared (IR) wavelength at 1064 nm and a pulse width of 5–7 ns. Analyses were carried out with beam energy in the range of 0·5–3 mJ per pulse. The ICPMS system is an Agilent 7500. The NIST 610 and 612 glasses were used as external standards; internal standards were CaO for diopside and garnet, and MgO for olivine. Data were reduced using the in-house GLITTER on-line software (van Achterbergh *et al.*, 2001), which provides for selection of stable intervals in each time-resolved analysis. Detection limits are typically less than 0·02 ppm for the rare earth elements (REE), Y, Nb, Ta, Th and U. The precision and accuracy of these analyses are 0·5–2% for REE, Y, Sr, Nb, Ta, Th and U at the ppm concentration level.

MINERAL CHEMISTRY

Olivine and enstatite

Olivine and enstatite in the Paleozoic Mengyin xenoliths or xenocrysts are highly magnesian with mean Mg-number of 92·4 ± 0·3 (1σ) and 93·5 ± 0·3, respectively. The mean Mg-number of olivine from depths of 150–175 km, calculated from garnet xenocrysts (n = 40) by the method of Gaul *et al.* (2000), is 92·2 ± 1·1. However, the Mg-numbers of olivine and enstatite in the Neogene Shanwang peridotites are lower, with a mean value of 89·5 ± 0·5 and 90·2 ± 0·3, respectively. Mg-numbers of olivine and enstatite in the CCSD-PP1 peridotites from the Sulu UHP terrane are intermediate (mean 91·7 ± 0·4 and 92·5 ± 0·3, respectively) between those of the Mengyin and Shanwang xenoliths (Fig. 3).

Mengyin olivines (xenoliths and xenocrysts, Tables 3 and 6) contain 650–780 ppm Ca, 2127–2633 ppm Ni, and 104–119 ppm Co. Shanwang olivines have slightly lower Ca (414–591 ppm) and similar Ni (∼2250 ppm) and Co (110–130 ppm). The olivines from the CCSD-PP1 UHP peridotites have still lower Ca (135–408 ppm) and Cr (4·01–20·1 ppm), but higher Sc (mean 4·93 ppm), Ni (2625–3376 ppm), Co (129–159 ppm) and Zn (33·9–71·4 ppm) contents than those of the xenoliths (Table 6).

Mengyin enstatites show a wide range in Al_2O_3 content (0·23–4·15 wt %). Shanwang enstatite has higher Al_2O_3 (3·51–6·10 wt %). The enstatites from the CCSD-PP1 peridotites have lower Al_2O_3 contents than the xenoliths from either area (Fig. 4a).

Diopside

Mengyin diopsides have a wide range of Na_2O (0·02–3·38 wt %), low Al_2O_3 and TiO_2, and high Ni (379–464 ppm), Mg-number (91·8–94·6) and Cr-number (22·4–46·9) (Fig. 4b). Shanwang diopsides have markedly high Al_2O_3 (5·75–7·87 wt %) and TiO_2 (0·36–0·57 wt %)

Downloaded from http://petrology.oxfordjournals.org/ at University of New Orleans on June 26, 2014

Table 1: Modes and electron microprobe analyses of minerals in garnet peridotite xenoliths from the North China Craton (wt %)

Occurrence:	Paleozoic xenoliths								Cenozoic xenoliths									
Locality:	Mengyin								Shanwang									
Rock type:	MY0211 Grt peridotite				MY0278 Grt peridotite				SW0169 Sp–Grt lherzolite					SW0193 Sp–Grt lherzolite				
Microstructure:	Porphyroclastic				Porphyroclastic				Porphyroclastic					Sheared				
Mineral:	Grt	Ol	Opx	Cpx	Grt	Ol	Opx	Cpx	Gnt	Ol	Opx	Cpx	Sp	Gnt	Ol	Opx	Cpx	Sp
Mode (%):	n.a.	n.a.	n.a.	n.a	n.a	n.a	n.a	n.a	2·1	53·5	24·2	17·7	2·5	1·2	54·9	27·7	13·5	2·9
No. of analyses:	5	5	5	5	5	5	5	5	5	5	5	5	5	5	5	5	5	3
SiO_2	41·2	41·7	58·9	55·7	41·9	40·7	57·2	54·9	42·3	41·0	55·4	52·7	0·06	42·2	40·6	55·2	52·5	0·09
TiO_2	0·09	0·00	0·00	0·01	0·43	0·01	0·04	0·12	0·18	0·01	0·09	0·36	0·10	0·15	0·01	0·05	0·40	0·13
Al_2O_3	16·2	0·03	0·54	1·09	19·5	0·02	0·44	1·51	22·1	0·02	4·37	6·20	57·3	22·8	0·02	4·15	6·62	52·7
Cr_2O_3	9·86	0·05	0·54	0·77	4·59	0·06	0·24	1·67	1·98	0·01	0·53	1·04	9·49	1·00	0·01	0·40	0·77	13·27
FeO	6·55	7·06	4·16	1·86	7·25	7·72	4·68	2·49	6·61	9·98	6·23	3·09	10·2	7·05	10·1	6·37	2·64	11·6
MnO	0·26	0·10	0·10	0·08	0·29	0·08	0·15	0·09	0·24	0·13	0·12	0·09	0·00	0·22	0·15	0·15	0·07	0·01
MgO	21·0	50·7	35·5	18·3	21·2	51·0	35·9	18·0	21·0	49·3	32·8	15·6	21·0	21·2	49·2	33·2	15·0	20·0
CaO	4·93	0·02	0·25	21·8	5·18	0·04	0·57	18·5	5·41	0·06	0·89	19·0	0·01	4·98	0·07	0·64	19·7	0·02
Na_2O	0·00	0·01	0·00	0·75	0·00	0·01	0·15	1·56	0·05	0·01	0·12	1·83	0·01	0·03	0·01	0·14	1·93	0·00
K_2O	0·00	0·00	0·00	0·10	0·00	0·00	0·00	0·06	0·00	0·00	0·00	0·00	0·00	0·00	0·00	0·00	0·00	0·00
NiO	0·00	0·37	0·10	0·02	0·00	0·35	0·18	0·04	0·03	0·36	0·12	0·06	0·40	0·10	0·41	0·13	0·08	0·29
Total	100·0	100·1	100·1	100·4	100·3	100·0	99·6	99·0	99·8	100·8	100·6	99·8	98·5	99·7	100·6	100·4	99·7	98·1
Mg-no.	85·1	92·8	93·8	94·6	83·9	92·2	93·2	92·8	85·0	89·8	90·4	90·0	78·6	84·3	89·7	90·3	91·0	75·5
Cr-no.	29·0	57·5	40·1	32·3	13·6	65·1	26·8	42·6	5·7	25·6	7·5	10·1	10·0	2·9	28·5	6·1	7·2	14·5

Occurrence:	Cenozoic xenoliths																	
Locality:	Shanwang																	
Rock type:	SW01-1 Grt lherzolite				SW01-8 Grt lherzolite				SW04-2 Sp–Grt lherzolite					SW04-6 Sp–Grt lherzolite				
Microstructure:	Sheared				Sheared				Fine-grained					Fine-grained				
Mineral:	Grt	Ol	Opx	Cpx	Grt	Ol	Opx	Cpx	Grt	Ol	Opx	Cpx	Sp	Grt	Ol	Opx	Cpx	Sp
Mode (%):	1·5	56·6	32·2	9·7	2·1	56·2	30·1	11·6	2·3	55·1	28·3	14·5	2·1	1·8	52·8	29·5	12·7	3·2
No. of analyses:	5	5	5	5	5	5	5	5	5	5	5	5	4	5	5	5	5	4
SiO_2	42·3	40·7	54·3	51·7	42·0	40·6	54·8	51·6	42·4	40·7	54·1	52·1	0·1	42·5	40·4	53·6	51·5	0·1
TiO_2	0·16	0·01	0·08	0·44	0·19	0·01	0·19	0·57	0·20	0·02	0·19	0·37	0·18	0·20	0·00	0·16	0·55	0·25
Al_2O_3	23·0	0·05	4·83	7·36	23·2	0·05	4·70	7·87	22·9	0·05	5·99	5·75	57·5	23·3	0·04	5·97	7·84	45·1
Cr_2O_3	0·76	0·02	0·70	0·68	0·62	0·02	0·56	0·39	0·54	0·02	0·27	1·25	8·12	0·48	0·00	0·34	0·58	20·2
FeO	7·22	10·2	5·83	3·33	7·65	11·1	6·39	3·70	7·91	11·3	7·01	2·99	10·7	7·91	11·5	6·71	3·70	12·4
MnO	0·28	0·16	0·10	0·09	0·28	0·14	0·12	0·09	0·33	0·15	0·12	0·10	0·01	0·32	0·16	0·13	0·10	0·00
MgO	21·3	49·4	32·3	15·9	21·2	48·6	32·4	15·8	21·2	48·6	31·5	16·1	21·4	21·3	47·1	31·6	15·7	19·5
CaO	5·12	0·09	1·13	18·6	4·89	0·10	1·00	18·0	4·90	0·09	1·04	19·2	0·00	4·94	0·11	1·12	17·8	0·01
Na_2O	0·02	0·02	0·12	1·62	0·02	0·02	0·18	1·81	0·02	0·01	0·21	1·54	0·00	0·02	0·02	0·19	1·81	0·01
K_2O	0·01	0·01	0·01	0·01	0·00	0·00	0·00	0·01	0·01	0·00	0·00	0·01	0·01	0·00	0·00	0·00	0·01	0·01
NiO	0·01	0·41	0·13	0·06	0·02	0·39	0·13	0·07	0·03	0·39	0·11	0·08	0·42	0·02	0·45	0·14	0·08	0·31
Total	100·1	101·0	99·5	99·7	100·1	101·0	100·5	99·9	100·5	101·3	100·5	99·4	98·3	101·0	99·7	99·9	99·6	97·9
Mg-no.	84·0	89·6	90·8	89·4	83·2	88·7	90·0	88·4	82·7	88·4	88·9	90·6	78·1	82·7	88·0	89·3	88·3	73·7
Cr-no.	4·1			10·7	3·3			6·0	3·0			21·9	15·4	2·6			8·7	36·7

Modal compositions of the Cenozoic xenoliths were obtained by counting more than 1500 points in each section. Modes are not given for Paleozoic xenoliths because of their strong alteration (n.a.).

Downloaded from http://petrology.oxfordjournals.org/ at University of New Orleans on June 26, 2014

Table 2: Modes and electron microprobe analyses of minerals in garnet peridotites at CCSD-PP1 from the Sulu UHP terrane (wt %)

Rock type:	ZMF2 Harzburgite			ZMF3 Lherzolite								ZMF4 Lherzolite					
Depth (m):	165			170								183					
Microstructure:	Sheared			Sheared								Sheared					
Mineral:	Grt	Ol	Opx	Grt	Grt	Ol	Opx	Cpx	Cpx	Cpx	Phl	Grt	Ol	Opx	Cpx	Sp	Phl
Mode (%):	3·5	62·6	33·9	3.3		59·0	30·2	5·3			2·2	3·8	57·9	29·2	5·6	0·5	3·0
No. of analyses:	5	5	5	core	rim	5	5	core	mantle	rim	4	5	5	5	5	4	4
SiO_2	41·5	41·4	58·4	41·3	41·0	41·2	58·0	54·6	54·9	54·3	42·0	41·4	41·1	58·5	54·9	0·03	41·9
TiO_2	0·02	0·00	0·01	0·01	0·01	0·00	0·01	0·01	0·01	0·00	0·05	0·00	0·02	0·01	0·01	0·03	0·09
Al_2O_3	21·0	0·01	0·18	21·2	20·8	0·01	0·19	1·14	1·23	1·20	12·4	21·6	0·01	0·16	1·23	17·1	12·6
Cr_2O_3	3·17	0·02	0·06	2·67	3·11	0·01	0·05	1·89	1·27	1·12	0·37	2·24	0·00	0·05	1·27	43·8	0·37
FeO	11·3	7·86	5·19	11·4	11·1	7·86	5·01	2·05	2·03	2·00	2·28	11·4	8·00	5·18	2·03	26·8	2·67
MnO	0·73	0·09	0·10	0·72	0·72	0·07	0·12	0·06	0·02	0·04	0·00	0·65	0·10	0·10	0·02	0·00	0·00
MgO	18·7	50·5	36·4	19·0	19·0	50·3	36·2	16·1	16·2	16·4	26·2	18·2	50·0	36·3	16·2	8·55	26·2
CaO	4·63	0·01	0·09	4·06	4·29	0·00	0·08	22·0	22·5	22·6	0·01	5·16	0·01	0·08	22·5	0·12	0·03
Na_2O	0·00	0·00	0·00	0·02	0·02	0·00	0·01	1·88	1·63	1·47	0·62	0·01	0·01	0·01	1·63	0·02	0·47
K_2O	0·00	0·00	0·00	0·00	0·00	0·00	0·00	0·01	0·01	0·00	8·98	0·01	0·01	0·00	0·01	0·00	8·51
NiO	0·04	0·34	0·01	0·04	0·03	0·32	0·02	0·01	0·02	0·04	0·05	0·03	0·38	0·05	0·06	0·02	0·04
Total	101·0	100·2	100·4	100·4	100·1	99·8	99·7	99·8	99·8	99·3	92·9	100·7	99·7	100·4	99·9	96·5	92·9
Mg-no.	74·6	92·0	92·6	74·8	75·3	91·9	92·8	93·3	93·4	93·6	95·3	74·0	91·8	92·6	93·4	36·2	94·6
Cr-no.	9·3			7·8	9·1			52·6	41·0	38·4		6·5			41·0	63·2	

Rock type:	ZMF6 Lherzolite								ZMF7 Lherzolite										
Depth (m):	184								193										
Microstructure:	Porphyroblastic								Porphyroblastic										
Mineral:	Grt	Grt	Grt	Ol	Opx	Cpx	Cpx	Sp	Grt	Grt	Grt	Ol	Opx	Cpx	Sp	Phl	Ol	Opx	Sp
Mode (%):	6·8			58·3	28·6	5·9		0·4	6·2			57·1	27·7	5·4	0·3	3·3			
No. of analyses:	core	rim	matrix	5	5	core	rim	4	core	rim	matrix	5	5	5	4	4	in Grt	in Grt	in Grt
SiO_2	41·9	41·7	41·2	41·2	58·3	54·9	54·8	0·01	41·7	41·5	41·5	41·1	58·3	54·4	0·05	41·6	40·9	58·1	0·00
TiO_2	0·01	0·01	0·02	0·00	0·00	0·01	0·00	0·61	0·04	0·00	0·00	0·00	0·01	0·01	0·14	0·10	0·00	0·00	0·28
Al_2O_3	22·0	21·9	19·6	0·01	0·17	1·07	1·05	4·0	22·0	22·0	21·8	0·01	0·16	1·00	7·85	13·0	0·00	0·24	6·48
Cr_2O_3	2·37	2·24	4·84	0·01	0·04	1·76	0·94	42·5	2·23	1·92	1·93	0·01	0·08	1·08	41·1	0·37	0·00	0·21	46·4
FeO	9·05	9·11	11·4	7·74	5·36	2·07	1·86	42·3	7·95	11·1	11·1	8·22	5·22	2·07	42·2	2·53	8·13	5·34	37·2
MnO	0·45	0·41	0·60	0·08	0·14	0·04	0·04	0·00	0·39	0·76	0·82	0·08	0·13	0·04	0·20	0·01	0·05	0·13	0·00
MgO	20·0	20·0	18·0	50·2	36·0	16·0	16·7	5·17	20·7	19·2	19·0	49·9	36·0	16·5	3·8	25·7	50·0	36·0	5·5
CaO	4·86	4·86	5·05	0·01	0·09	22·0	23·1	0·05	5·03	3·82	4·22	0·00	0·09	22·7	0·00	0·01	0·00	0·09	0·00
Na_2O	0·01	0·01	0·02	0·00	0·02	1·88	1·25	0·00	0·01	0·01	0·00	0·00	0·01	1·34	0·00	0·60	0·01	0·02	0·00
K_2O	0·00	0·00	0·01	0·00	0·01	0·00	0·00	0·00	0·00	0·01	0·00	0·01	0·01	0·01	0·01	8·93	0·00	0·00	0·00
NiO	0·02	0·02	0·01	0·34	0·01	0·02	0·01	0·00	0·01	0·01	0·02	0·37	0·00	0·02	0·03	0·35	0·35	0·03	0·04
Total	100·7	100·3	100·6	99·5	100·2	99·7	99·8	94·7	100·0	100·3	100·3	99·6	100·0	99·2	95·4	93·1	99·4	100·1	95·9
Mg-no.	79·7	79·6	73·8	92·0	92·3	93·2	94·1	17·9	82·3	75·5	75·2	91·5	92·5	93·4	13·9	94·8	91·6	92·3	20·9
Cr-no.	6·7	6·4	14·2			52·5	37·7	87·8	6·4	5·5	5·6			42·2	77·8				82·8

Downloaded from http://petrology.oxfordjournals.org/ at University of New Orleans on June 26, 2014

Table 2: *continued*

Rock type:	ZMF8 Lherzolite							ZMF11 Harzburgite				ZML Lherzolite							
Depth (m):	209							254				?							
Microstructure:	Porphyroblastic							Sheared				Porphyroblastic							
Mineral:	Grt	Grt	Ol	Opx	Cpx	Cpx	Cpx	Ol	Opx	Sp	Phl	Grt	Grt	Grt	Ol	Ol	Ol	Opx	Cpx
Mode (%):	5·2		58·2	30·9	5·7			70·8	26·4	0·3	2·5	6·7			59·8			27·3	6·2
No. of analyses:	core	rim	5	5	core	mantle	rim	5	5	4	4	core	rim	matrix	core	rim	in Cpx	5	5
SiO_2	42·0	42·0	41·0	58·0	54·3	54·2	54·2	40·8	58·9	0·01	40·1	41·5	41·6	41·0	40·2	40·2	40·4	58·1	55·1
TiO_2	0·01	0·00	0·00	0·01	0·00	0·01	0·03	0·00	0·01	0·19	0·05	0·13	0·06	0·00	0·00	0·00	0·05	0·02	0·01
Al_2O_3	22·2	22·4	0·00	0·19	1·42	1·62	1·45	0·01	0·18	2·81	10·7	22·9	22·1	21·9	0·01	0·03	0·01	0·25	1·61
Cr_2O_3	1·89	1·44	0·01	0·05	1·74	1·46	1·20	0·00	0·05	48·2	0·23	1·60	1·71	2·29	0·01	0·03	0·00	0·08	1·25
FeO	9·70	10·4	7·71	5·01	2·09	2·28	2·12	9·16	5·19	39·9	3·52	8·24	10·5	11·5	8·72	8·13	8·56	5·59	2·80
MnO	0·45	0·62	0·08	0·12	0·03	0·04	0·01	0·18	0·11	0·42	0·03	0·27	0·59	0·51	0·09	0·03	0·08	0·11	0·03
MgO	19·7	19·3	50·3	36·2	15·9	15·8	16·3	49·2	36·5	3·12	29·5	20·4	18·9	19·0	50·8	51·1	51·4	36·2	15·5
CaO	4·83	4·66	0·00	0·08	21·8	21·7	22·3	0·00	0·08	0·01	0·01	5·09	4·70	3·88	0·03	0·02	0·02	0·07	20·9
Na_2O	0·03	0·02	0·01	0·01	1·88	1·98	1·64	0·00	0·00	0·02	0·07	0·05	0·03	0·03	0·00	0·00	0·02	0·02	2·34
K_2O	0·00	0·01	0·00	0·00	0·00	0·01	0·00	0·00	0·00	0·00	6·70	0·01	0·00	0·01	0·02	0·00	0·02	0·00	0·02
NiO	0·02	0·04	0·37	0·02	0·03	0·04	0·01	0·35	0·02	0·02	0·05	0·00	0·02	0·00	0·44	0·47	0·40	0·12	0·01
Total	100·8	100·9	99·6	99·7	99·1	99·2	99·3	99·8	101·0	94·8	91·0	100·1	100·3	100·2	100·3	99·9	100·9	100·6	99·6
Mg-no.	78·3	76·8	92·1	92·8	93·1	92·5	93·2	90·5	92·6	12·2	93·7	81·5	76·2	74·6	91·2	91·8	91·5	92·0	90·8
Cr-no.	5·4	4·1			45·1	37·6	35·7			92·0		4·5	5·0	6·6					34·3

Data on sample ZML after Zheng *et al*. (2005*a*).

and relatively low Ni (308–405 ppm), Mg-number (88·3–91·0) and Cr-number (6·0–21·9). The diopsides of the CCSD-PP1 peridotites have similar Na_2O, Al_2O_3 and TiO_2 contents (Fig. 4c and d) to the Paleozoic Mengyin xenoliths or xenocrysts, but lower Ni (222–256 ppm).

Mengyin diopsides have 21·0–46·6 ppm REE, 0·68–0·73 ppm heavy REE (HREE) and $(La/Yb)_n$ of 12·5–16·5. Shanwang diopsides are high in HREE (2·35–4·79 ppm), and have low $(La/Yb)_n$ (2·6–3·3) compared with those from Mengyin. The diopsides of the CCSD-PP1 peridotites have lower HREE (<0·40 ppm), and higher $(La/Yb)_n$ (80·3–143), than diopsides from either set of xenoliths. The primitive mantle-normalized REE patterns of the Mengyin diopsides are HREE-depleted with strong enrichment from Dy to La. Shanwang diopsides show flat REE patterns (Fig. 5). However, the REE patterns of the diopside in the CCSD-PP1 peridotites vary widely, from sinusoidal (e.g. sample ZML; Zheng *et al.*, 2005*a*) to light REE (LREE)-enriched, exhibiting strong HREE depletion from Lu to Ho or Eu with LREE enrichment from Dy or Sm to La.

Relative to primitive mantle (see Fig. 5), Mengyin diopsides have high contents of the incompatible trace elements except Nb, Zr, Ti and HREE, and hence negative Nb, Zr, Ti and Th anomalies, but positive Sr and U anomalies. Shanwang diopsides have lower Ba contents, but higher Y, Th, U, Ti, Zr, Hf and Nb than Mengyin diopsides, and show weak to strong negative Zr, Nb and Ti anomalies. The diopsides from the CCSD-PP1 peridotites have a wide range of Ba, and lower U, Th, Nb, Zr, Ti and Y contents, but higher Sr contents than Mengyin diopsides, and display distinctly negative Nb, Zr and Ti anomalies.

Garnet

Mengyin garnets are magnesian chrome-pyrope with a wide range of Cr_2O_3 contents (2·27–9·86 wt %) and Cr-number [Cr/(Cr + Al); 6·8–29·0]. Shanwang garnets have low Cr_2O_3 contents (0·48–1·98 wt %) and Cr-number (2·6–5·7). Garnets from the CCSD-PP1 peridotites are chrome-pyrope (1·44–3·17 wt % Cr_2O_3) with moderate amounts of grossular (mean 4·50 wt % CaO), and much lower Mg-number than the garnets from Mengyin (Fig. 6). In the garnets of three samples (ZMF6, -7 and -8), CaO and Cr_2O_3 decrease from the core to the rim of the porphyroblasts, but are higher again in the matrix garnets. However, in the garnet of sample

Downloaded from http://petrology.oxfordjournals.org/ at University of New Orleans on June 26, 2014

Table 3: Major and LAM–ICPMS trace element compositions of individual olivine xenocrysts from Mengyin kimberlites

	Grain no.						
	MY1	MY2	MY3	MY4	MY5	MY6	MY7
wt %							
SiO_2	41·0	40·6	40·8	40·7	41·0	40·7	40·7
TiO_2	0·00	0·01	0·02	0·05	0·00	0·03	0·00
Al_2O_3	0·01	0·01	0·01	0·00	0·04	0·00	0·01
Cr_2O_3	0·04	0·05	0·06	0·09	0·07	0·05	0·08
FeO	7·57	7·62	7·61	7·62	7·50	7·77	7·59
MnO	0·08	0·09	0·08	0·08	0·11	0·07	0·03
MgO	51·5	50·8	51·2	50·8	52·0	51·0	51·2
CaO	0·05	0·04	0·03	0·01	0·03	0·00	0·04
Na_2O	0·00	0·01	0·01	0·00	0·04	0·00	0·01
K_2O	0·00	0·01	0·01	0·00	0·00	0·00	0·02
NiO	0·46	0·46	0·35	0·17	0·36	0·28	0·34
Total	100·7	99·7	100·2	99·5	101·2	99·9	100·0
Mg-no.	92·4	92·2	92·3	92·2	92·5	92·1	92·3
ppm							
Ca	940	1605	1143	780	654	805	830
Sc	2·68	2·98	2·74	2·18	2·08	2·41	2·43
V	7·57	4·92	4·90	4·16	4·07	6·26	6·32
Co	119	104	105	117	117	106	106
Cr	199	349	352	311	309	253	255
Ni	2127	2340	2357	2612	2633	2278	2309
Mn	776	666	667	771	776	726	732

ZML, CaO decreases as Cr_2O_3 increases from the core through the rim of the porphyroblast and into the matrix (Zheng *et al.*, 2005*a*), suggesting that the garnet grew by subsolidus re-equilibration with spinel and diopside until the disappearance of spinel.

Mengyin garnets have 1·71–16·6 ppm Y, 8·21–137 ppm Zr, 10–12 ppm REE, and $(La/Yb)_n = 0{\cdot}06$–0·07; they show depleted LREE and flat HREE from Sm to Lu (Fig. 7). Shanwang garnets contain 30–100 ppm Y, 25–58 ppm REE and $(La/Yb)_n = 0{\cdot}02$–0·17; the REE pattern is weakly convex upward and has a negative Ce anomaly. Garnets from the CCSD-PP1 peridotites are low in REE (4·78–23·1 ppm) and have strongly negative Ce anomalies [$\delta Ce = 0{\cdot}27$–0·61, where δCe defined as $2 \times Ce_n/(La_n + Pr_n)$].

Phlogopite

Phlogopite in four CCSD-PP1 peridotites (Tables 2 and 7) has 15·1–20·7 Mg/Fe, low TiO_2 (<0·10 wt %), and high Ba (5800–10 000 ppm), Ni (1120–1500 ppm) and Nb (1·11–4·18 ppm), suggesting a metasomatic origin (Fig. 2f).

P–T ESTIMATES

P–T conditions (Table 8; Fig. 8) were estimated using a combination of the Grt–Opx barometer based on Al partitioning (Brey & Kohler, 1990) and the Grt–Cpx (Krogh Ravna, 2000) and Grt–Opx (O'Neill & Wood, 1979) Fe–Mg exchange thermometers. In the xenolith samples, where the phases are homogeneous, we have combined the average compositions given in Table 1. Estimated *P–T* conditions for the two Paleozoic Mengyin xenoliths are 56–60 kbar and ~1100°C, and fall near a conductive model geotherm corresponding to a surface heat flow of 40 mW/m^2. The Cenozoic garnet peridotite xenoliths from Shanwang give estimates of 16–24 kbar and 1000–1180°C and fall near a 80 mW/m^2 conductive model. The estimates for the Shanwang xenoliths overlap the range of values derived for garnet peridotite xenoliths from the Nushan area (CTG; Xu *et al.*, 1998, 2000). The estimated *P–T* conditions of the CCSD-PP1 peridotites, in which the minerals (especially garnet and clinopyroxene) are commonly zoned, have been estimated by combining core–core, rim–rim and matrix pairs. The estimates from the cores range from 660 to 770°C and from 31 to 53 kbar. The cores of large garnets and pyroxenes (e.g. porphyroblasts) in samples ZMF6, ZMF7 and ZML give slightly higher temperatures (by 5–40°C) and pressures (by 1·5–12 kbar) than the minerals of the matrix or the rims of the porphyroblasts. These estimates fall well below the typical conductive geotherms found in cratonic lithosphere. The samples from this study appear to be derived from shallower depths than those studied by Yang *et al.* (1993), Zhang *et al.* (1995, 2000, 2003) and Yang & Jahn (2000), and the *P–T* estimates suggest a geotherm that is steeper than the 40 mW/m^2 conductive model.

Ni temperatures (T_{Ni}, Ryan *et al.*, 1996) of the garnets range from 1157 to 1215°C for the Paleozoic xenoliths, and from 1145 to 1196°C for the Cenozoic xenoliths. Zoning studies (Ryan *et al.*, 1996) show that the Ni-in-garnet thermometer equilibrates very rapidly in response to changes in temperature. Most of the T_{Ni} estimates are within the ±50°C uncertainties of the BK90 (Brey & Kohler, 1990) estimates (Table 8), but several are higher by up to 190°C, suggesting late-stage heating of the xenoliths prior to eruption. In the CCSD-PP1 peridotites the method gives 662–845°C for garnet cores, and 569–718°C for rims of garnet. Most of these temperatures are 80–240°C lower than the estimates from the mineral pairs, and may record cooling during exhumation of the peridotite to crustal depths (Table 8). The temperatures of the Paleozoic garnet xenocrysts show a similar range

Downloaded from http://petrology.oxfordjournals.org/ at University of New Orleans on June 26, 2014

Table 4: Major and LAM–ICPMS trace element compositions of individual garnet xenocrysts from Mengyin kimberlites

Grain no.	SD50	SD51	SD52	SD53	SD54	SD55	SD57	SD58	SD59	SD60	SD62	SD63	SD64	SD65	SD66	SD67	SD68	SD69	SD70	SD71	SD72	SD73	SD74	SD75
wt %																								
SiO_2	42·5	42·6	42·0	42·5	42·4	42·0	42·1	42·6	42·1	42·3	41·9	42·5	42·0	41·9	42·0	41·7	41·8	41·7	41·7	41·2	42·0	41·8	41·3	41·6
TiO_2	0·41	0·49	0·72	0·44	0·62	0·60	0·60	0·36	0·61	0·60	0·57	0·49	0·25	0·22	0·57	0·60	0·57	0·52	0·53	0·63	0·12	0·18	0·59	0·36
Al_2O_3	20·0	20·0	20·1	20·0	21·0	20·7	20·9	20·3	20·9	20·9	19·9	19·9	18·6	19·7	17·4	17·4	17·6	17·4	17·8	18·2	18·7	18·5	18·3	18·5
Cr_2O_3	3·31	3·20	3·40	3·40	2·29	2·28	2·56	3·32	2·27	2·49	3·20	3·06	5·34	4·88	6·65	7·16	6·81	6·79	6·87	6·15	6·44	6·31	6·28	6·33
FeO	6·97	7·04	7·72	6·87	8·01	8·03	8·43	7·07	8·28	8·42	7·63	7·01	6·46	6·14	6·39	6·38	6·44	6·54	6·37	7·36	6·80	7·18	7·32	7·17
MnO	0·27	0·26	0·31	0·30	0·35	0·31	0·31	0·26	0·22	0·25	0·36	0·21	0·25	0·24	0·21	0·22	0·24	0·23	0·17	0·27	0·18	0·33	0·26	0·33
MgO	22·0	22·3	21·2	22·1	21·0	21·3	21·3	22·3	20·8	21·1	21·1	22·0	21·9	21·6	21·1	21·1	21·5	21·2	21·2	21·0	21·0	21·3	20·8	21·3
CaO	4·75	4·80	5·39	4·72	5·03	5·06	5·01	4·69	4·90	5·05	5·33	4·81	5·33	5·10	5·34	5·49	5·46	5·46	5·46	4·98	5·22	5·03	5·14	5·09
Total	100·1	100·7	100·7	100·3	100·7	100·3	101·2	100·9	100·1	101·0	100·0	100·0	100·2	99·8	99·6	100·0	100·4	99·8	100·0	99·8	100·3	100·6	100·0	100·6
Mg-no.	84·9	85·0	83·0	85·1	82·4	82·5	81·8	84·9	81·8	81·7	83·1	84·8	85·8	86·3	85·5	85·5	85·6	85·2	85·6	83·6	84·6	84·1	83·5	84·1
Cr-no.	10·0	9·7	10·2	10·2	6·8	6·9	7·6	9·9	6·8	7·4	9·7	9·3	16·1	14·2	20·4	21·7	20·6	20·7	20·6	18·5	18·8	18·6	18·7	18·7
ppm																								
Sc	103	103	116	103	100	56·7	116	104	96·2	97·4	110	105	115	125	119	172	118	119	120	141	145	141	150	145
Ti	2796	3052	4160	2801	3787	1974	2445	2582	3707	3797	4150	2819	1909	1100	3480	4296	3550	3547	3479	3443	838	1228	3824	2567
V	246	256	322	235	311	155	255	241	299	309	322	254	328	334	319	417	323	324	319	310	350	325	293	329
Co	43·2	43·5	44·0	42·4	43·7	50·4	46·2	45·5	46·6	44·5	44·3	45·2	46·1	36·2	41·6	61·9	41·4	41·2	41·4	40·2	38·9	38·7	41·3	38·5
Ni	53·8	57·9	56·5	56·5	53·1	37·2	58·6	57·9	59·2	57·3	60·1	59·8	65·0	45·1	51·8	76·1	51·9	51·4	51·4	75·8	72·0	72·5	78·4	73·8
Ga	8·19	8·63	11·6	8·63	12·2	9·75	9·40	8·84	12·4	12·9	12·3	9·22	11·1	5·80	11·0	11·8	11·4	11·2	11·3	6·58	6·46	6·04	5·53	6·32
Sr	0·72	0·86	0·73	0·89	0·36	0·44	1·07	0·68	0·38	<0·48	0·49	0·78	1·63	<0·48	1·13	12·59	1·35	1·24	1·38	1·01	0·82	0·92	1·17	1·10
Y	14·6	15·3	16·6	15·1	14·8	15·6	16·6	14·5	13·8	14·7	16·3	14·6	11·18	4·07	13·5	20·1	13·9	14·1	14·0	3·09	3·29	2·72	2·94	2·83
Zr	57·4	68·4	69·6	59·4	62·1	6·95	42·0	47·2	59·2	61·9	67·8	59·1	33·8	25·6	93·5	137	98·0	99·7	96·6	84·2	8·21	14·7	88·1	58·5
Hf	1·28	1·79	2·11	1·61	1·62	<0·35	0·87	1·49	1·87	1·63	1·94	1·46	0·97	<0·91	2·30	2·92	2·03	2·39	2·20	1·37	<0·71	<0·80	1·43	1·18
Nb	0·78	0·70	0·74	0·47	0·41	<0·29	<0·44	0·89	<0·53	<0·47	0·73	0·91	0·91	<0·57	0·94	1·30	0·90	1·07	0·85	0·62	<0·59	<0·58	0·59	<0·53
Ce	1·17	1·18	0·47	1·19	0·27	0·21	1·17	1·14	0·21	0·29	0·50	0·95	1·41	0·53	0·89	4·24	0·65	0·89	0·95	0·75	0·86	0·84	0·55	0·83
Nd	2·84	2·58	<1·20	2·20	1·30	<0·81	2·73	2·77	<0·97	<1·30	<1·41	3·00	4·05	3·08	3·20	5·70	2·42	2·47	2·77	2·55	2·34	2·04	2·66	2·61
Eu	0·53	<0·30	0·46	0·62	0·28	0·22	0·41	0·41	0·39	0·40	0·40	0·68	0·45	0·44	<0·67	0·97	0·93	0·97	0·88	0·43	<0·43	<0·54	<0·52	<0·42
Dy	2·34	1·82	2·88	2·10	2·93	1·84	1·88	1·69	2·22	2·77	3·02	2·47	1·83	<1·19	2·40	2·45	1·86	2·57	3·31	0·93	<1·25	<1·47	<1·30	<1·16
Ho	0·53	0·56	0·62	0·52	0·65	0·60	0·64	0·65	0·49	0·51	0·55	0·58	0·35	0·31	0·73	0·58	0·53	0·58	0·46	<0·15	<0·26	<0·25	<0·27	0·23
Mn																								
T_{Ni} (°C)	1056	1080	1072	1072	1051	943	1085	1080	1088	1077	1093	1092	1122	999	1043	1182	1043	1041	1040	1180	1160	1163	1194	1170
P_{Cr} (kbar)	37·0	36·7	34·6	37·6	29·0	27·4	31·8	37·3	29·3	30·2	34·0	36·0	44·2	38·9	47·4	49·4	47·6	47·4	47·3	44·9	44·5	44·9	44·8	45·0

P–T conditions are estimated by the method of Ryan *et al.* (1996). P_{Cr} estimates are minimum values.

Downloaded from http://petrology.oxfordjournals.org/ at University of New Orleans on June 26, 2014

Table 5: LAM–ICPMS trace element analyses of individual diopside xenocrysts from Mengyin kimberlites (ppm)

	Grain no.											
	SD1	SD2	SD3	SD4	SD5	SD6	SD8	SD9	SD10	SD11	SD12	SD13
wt %												
SiO_2	55·4	55·1	55·7	55·0	54·8	55·6	55·1	55·3	54·5	55·1	54·7	54·9
TiO_2	0·14	0·19	0·15	0·03	0·18	0·04	0·25	0·12	0·34	0·19	0·21	0·18
Al_2O_3	1·45	1·46	1·40	1·25	1·56	1·05	1·45	1·25	1·53	1·42	1·53	1·58
Cr_2O_3	1·53	1·30	1·84	1·42	0·67	1·05	1·29	1·52	1·63	1·24	1·65	1·10
FeO	2·44	2·96	2·41	2·27	2·77	1·99	2·48	2·54	2·52	2·62	2·41	2·90
MnO	0·07	0·18	0·07	0·11	0·14	0·09	0·08	0·16	0·08	0·06	0·07	0·14
MgO	18·5	18·9	17·9	18·5	19·0	18·7	18·2	18·9	18·4	18·3	18·3	18·3
CaO	18·3	18·2	18·1	19·8	19·0	20·2	18·9	18·3	18·5	19·0	19·1	19·0
Na_2O	1·52	1·48	1·61	1·26	1·46	1·11	1·53	1·49	1·64	1·33	1·40	1·32
K_2O	0·03	0·07	0·08	0·09	0·07	0·06	0·04	0·06	0·08	0·04	0·10	0·07
Total	99·4	99·9	99·2	99·8	99·7	99·8	99·4	99·6	99·2	99·3	99·5	99·5
Mg-no.	93·2	92·0	93·0	93·6	92·5	94·4	93·0	93·0	92·9	92·6	93·2	91·9
Cr-no.	42·3	38·2	47·8	44·2	22·9	41·0	38·3	45·8	42·5	37·7	42·8	32·6
ppm												
Sc	17·0	16·8	20·2	14·5	15·3	13·0	18·4	17·9	22·5	18·8	19·1	16·4
Ti	252	342	270	54	324	72	450	216	612	342	378	324
V	168	216	212	219	221	198	208	202	324	244	223	227
Co	24·2	26·3	22·0	22·0	26·6	24·5	24·5	23·9	23·1	24·3	23·8	26·6
Ni	426	440	379	389	453	464	437	425	406	418	405	463
Sr	197	298	183	334	165	402	166	183	157	165	189	190
Y	2·06	2·62	2·14	0·35	1·93	0·33	2·22	1·53	3·65	2·43	1·84	2·04
Zr	8·37	22·4	7·18	3·90	5·04	5·26	6·57	4·52	15·3	7·68	6·78	5·83
Nb	0·70	0·37	<0·27	2·13	0·47	0·48	0·42	0·35	0·54	0·44	0·62	1·08
La	4·12	4·33	2·70	6·53	2·72	4·25	2·57	2·63	3·07	2·78	3·21	3·13
Ce	9·50	16·3	9·06	19·9	8·56	14·8	7·46	8·30	10·1	8·94	9·27	9·03
Pr	1·62	3·02	1·61	3·17	1·53	2·92	1·25	1·27	1·68	1·33	1·71	1·50
Nd	6·76	15·8	6·62	13·2	7·27	16·4	5·81	6·94	9·88	6·97	7·82	5·32
Sm	1·37	3·76	1·99	1·59	1·87	2·83	1·53	<1·03	1·79	1·99	1·41	1·08
Eu	0·48	0·85	<0·36	0·40	0·30	0·44	0·35	<0·23	0·51	0·54	0·46	0·41
Gd	1·11	1·37	2·01	1·10	<0·86	0·84	0·96	<0·81	2·08	<1·17	<1·07	1·00
Tb	0·17	0·14	0·13	0·15	0·13	0·09	0·07	0·07	0·15	0·04	0·09	0·08
Dy	0·73	0·58	0·40	0·56	0·38	0·38	0·30	0·25	0·60	0·22	0·33	0·09
Ho	0·12	0·07	0·04	0·08	0·07	0·05	0·04	0·02	0·07	0·03	0·05	0·02
Er	0·34	0·12	0·07	0·21	0·09	0·13	0·09	0·08	0·17	0·06	0·08	0·04
Tm	0·04	0·02	0·02	0·03	0·02	0·03	0·02	0·02	0·02	0·02	0·02	0·01
Yb	0·17	0·11	0·16	0·17	0·13	0·13	0·13	0·12	0·08	0·13	0·03	0·04
Lu	0·02	0·02	0·02	0·02	0·02	0·02	0·02	0·01	0·04	0·02	0·02	0·01
Hf	0·67	0·38	0·42	0·54	0·50	0·45	0·27	0·15	1·14	0·10	0·28	0·34
Th	0·20	0·03	0·04	0·12	0·05	0·14	0·22	0·08	0·08	0·29	0·10	0·07
U	0·19	0·02	0·02	0·11	0·02	0·25	0·15	0·03	0·03	0·04	0·04	0·03

Major element compositions from Zheng *et al.* (2005*c*).

Downloaded from http://petrology.oxfordjournals.org/ at University of New Orleans on June 26, 2014

Table 6: LAM–ICPMS trace element analyses of olivines in peridotites (ppm)

Sample	Mg-no.	Ca	Sc	V	Cr	Mn	Co	Ni	Zn
Mengyin, Paleozoic									
MY0211	92·8	780	2·18	4·16	311	771	117	2612	43·7
MY0278	92·2	654	2·08	4·07	309	776	117	2633	44·3
Shanwang, Cenozoic									
SW0169	89·8	414	3·07	2·08	41·5	1001	110	2263	49·6
SW0193	89·7	591	3·09	2·83	56·6	1091	130	2567	45·7
SW01-1	89·6	404	2·82	1·92	51·1	864	120	2523	37·3
SW01-8	88·7	439	2·79	2·15	57·3	920	125	2561	39·6
SW04-2	88·4	529	3·09	2·75	56·4	1091	130	2564	46·0
SW04-6	88·0	450	2·64	1·94	32·6	998	121	2517	27·1
CCSD-PP1, Mesozoic									
ZMF2	92·0	225	5·20	1·44	7·01	651	144	3367	50·8
ZMF3	91·9	333	4·65	2·33	9·66	666	151	3240	55·9
ZMF4	91·8	408	5·85	3·83	5·79	812	129	2625	43·9
ZMF6	92·0	354	5·31	7·00	4·01	790	159	3500	48·2
ZMF7	91·5	347	4·51	1·26	7·51	784	156	3315	60·8
ZMF8	92·1	379	4·72	1·02	4·71	681	148	3376	48·1
ZMF11	90·5	135	4·29	0·79	5·04	1459	147	2918	71·4
ZML	91·2	344	1·21	5·72	20·1	879	133	2809	43·9

Data on sample ZML after Zheng *et al.* (2005*a*).

to the peridotitic xenoliths (see Tables 4 and 8). P_{Cr} estimates for the xenocrysts, based on Cr_2O_3 contents (Ryan *et al.*, 1996), are minimum values, and thus are lower than the estimates for the xenoliths; a few grains give T_{Ni}–P_{Cr} estimates that lie along the same geotherm as the two xenoliths (MY0211 and MY0278).

DISCUSSION

Lithospheric thickness and thermal state

The Paleozoic kimberlite-hosted xenoliths are mainly refractory garnet peridotites (Griffin *et al.*, 1998*a*; Zheng & Lu, 1999). Silicate inclusions in diamonds (Zhang *et al.*, 1994) and garnet concentrates from the kimberlites yield a cool geotherm corresponding to a surface heat flow of ~40 mW/m^2 (Griffin *et al.*, 1998*a*; Zheng, 1999). These *P–T* estimates suggest that the Paleozoic lithosphere had stabilized to a depth of ~200 km, well within the diamond stability field (Griffin *et al.*, 1992, 1998*a*; Lu & Zheng, 1996). The *P–T* estimates (e.g. Brey & Kohler, 1990) for MY0211 and MY0278 (Fig. 8) are in good agreement with this geotherm, providing further evidence for a cool and thick lithosphere.

The Cenozoic basalt-hosted xenoliths from the North China Craton consist mainly of spinel peridotites (Fan & Hooper, 1989; Zheng *et al.*, 1998; Chen *et al.*, 2001) and rare garnet peridotites (Xu *et al.*, 1998, 2000; Zheng, 1999). Xu *et al.* (1998) used garnet pyroxenite and garnet peridotite xenoliths from this area to derive an elevated, strongly convex-upward geotherm similar to that calculated for xenolith suites from SE Australia (O'Reilly & Griffin, 1985). The *P–T* estimates for the Shanwang garnet peridotites plot near this geotherm, indicating a thinner and hotter lithosphere in the Cenozoic than in the Paleozoic (Fig. 8).

The *P–T* region with very low temperatures and high pressure (geothermal gradient $<5°C/km$) was once considered to be a 'forbidden zone' not reached in the Earth (Schreyer, 1988). However, it is now documented that some UHP rocks have been recrystallized at *P–T* conditions of the forbidden zone (Liou *et al.*, 2000). *T* estimates for the CCSD-PP1 peridotites, which have low-Ca olivine consistent with low temperature (O'Reilly *et al.*, 1996), are very low (~845–570°C), implying that they equilibrated in or near the forbidden zone (Fig. 8) during deep lithospheric subduction and UHP metamorphism. Ni temperatures for the porphyroblastic garnets decrease from core through rim to the matrix (Table 8). Considering the increase in Cr_2O_3 from the rim of porphyroblastic garnet to the matrix (Table 2), we suggest that the following reaction accompanied the deep subduction: diopside + enstatite + spinel + fluid → garnet + olivine + phlogopite. This reaction would produce a relatively high-Ni olivine, as observed in the CCSD-PP1 peridotites (Table 6).

Peridotite composition vs tectonic setting

The most distinctive feature of the Archean lithospheric mantle, which differentiates it from the lithospheric mantle beneath Phanerozoic terranes, is the presence of very depleted harzburgites with strongly subcalcic garnets (low Ca/Al); in the Kaapvaal Craton of Africa, and to a much lesser degree in the Siberian Craton, many such rocks have high Opx/Ol ratios reflecting low Mg/Si (Boyd, 1996). Subcalcic (Cpx-free) harzburgites are almost entirely restricted to Archean mantle; the dominant lherzolites become progressively less depleted from Archean through Proterozoic to Phanerozoic lithospheric mantle (Griffin *et al.*, 1998*b*). These differences also are observed between the Mengyin and Shanwang peridotites. The reconstructed bulk compositions of Mengyin peridotites have much lower CaO and Al_2O_3 contents (Zheng, 1999) but higher Mg-number values than commonly accepted primitive-mantle compositions (e.g. Hart & Zindler, 1986; McDonough & Sun, 1995). They are compositionally similar to the low-*T* peridotite xenoliths from kimberlites in the Kaapvaal Craton, reflecting a high degree of depletion in basaltic components (Boyd, 1996; Bernstein *et al.*, 1998). In contrast, most of the Shanwang peridotites are fertile

Downloaded from http://petrology.oxfordjournals.org/ at University of New Orleans on June 26, 2014

Table 7: Trace element concentrations of garnet and diopside in peridotites by LAM–ICPMS (ppm)

Locality:	Mengyin, Paleozoic xenolith				Shanwang, Cenozoic xenoliths																CCSD-PP1, Mesozoic UHP terrane							
Sample:	MY0211		MY0278		SW0169		SW0193		SW01-1		SW01-8		SW04-2		SW04-6		ZMF2			ZMF3					
Mineral:	Cpx	Grt	Cpx	Grt	Cpx	Grt	Cpx	Grt	Cpx	Grt	Cpx	Grt	Cpx	Grt	Cpx	Grt	Grt	Phl	Grt	Grt	Cpx	Cpx	Cpx	Phl
Average:	5	5	5	5	5	5	5	5	5	5	5	5	5	5	5	5	5	3	core	rim	core	mantle	rim	3
Sc	16·8	169	17·2	117	61·4	138	66·2	179	53·2	125	49·4	131	56·8	176	56·8	161	81·4	8·44	62·0	57·1	21·4	19·2	23·2	4·98
Ti	180	561	212	2554	2246	1325	2087	1687	2160	1405	2152	1250	1847	1615	1431	1567	55·3	304	161	113	52·3	54·3	65·7	483
V	207	385	224	291	266	128	249	130	251	143	221	129	286	113	292	129	64·7	35·1	104	95·8	490	467	448	71·4
Co	24·2	43·0	24·2	43·4	23·6	39·2	20·2	47·6	21·4	36·8	19·4	39·8	24·1	44·5	25·7	49·3	40·2	38·8	36·1	33·2	12·3	12·7	13·5	47·4
Ni	417	69·2	431	78·8	377	74·7	310	78·2	320	74·3	308	77·6	396	71·5	405	82·4	5·00	1161	10·1	5·39	222	243	239	1533
Sr	235	4·09	226	1·11	104	1·09	106	0·51	230	2·3	217	0·3	94·0	<0·81	62·3	0·36	2·27	99·6	0·20	0·14	1941	1192	1105	99·0
Y	1·82	1·71	1·99	12·4	13·1	37·2	13·8	86·2	20·4	30·4	17·2	49·5	13·0	100	9·87	68·7	5·31	0·29	12·4	14·0	1·33	1·13	1·27	0·14
Zr	9·38	12·9	9·64	55·8	43·9	28·6	28·6	59·8	145	24·6	101	28·4	19·1	63·5	12·4	51·1	1·43	1·56	15·7	12·9	5·21	6·59	8·13	1·82
Nb	0·79	0·58	0·57	0·65	1·65	0·69	0·72	0·66	2·00	1·22	2·38	<0·19	2·82	<1·25	1·66	0·55	0·07	1·36	0·26	0·09	0·07	0·05	0·14	4·81
Ba	5·02	<0·58	4·30	<0·83	3·01	<0·21	1·83	<0·19	n.a.	n.a.	n.a.	n.a.	n.a.	n.a.	n.a.	n.a.	0·39	8792	<0·97	<1·12	623	7·45	153	8731
La	4·08	0·09	3·27	0·11	3·62	0·79	4·71	0·34	7·99	1·79	7·27	<0·18	4·39	<0·47	2·01	<0·36	0·22	0·11	0·03	<0·59	17·6	15·4	13·9	<0·68
Ce	12·7	0·65	10·2	0·77	9·14	1·13	10·8	0·33	25·8	2·88	23·1	<0·16	7·22	<0·54	4·33	<0·28	0·33	0·46	0·25	0·20	51·1	45·8	44·1	0·06
Pr	2·19	0·21	1·77	0·21	1·54	0·28	1·44	0·26	4·12	0·42	3·61	<0·10	1·23	<0·41	0·64	<0·26	0·07	0·02	0·17	0·10	7·41	6·71	6·78	<0·05
Nd	9·93	1·54	8·96	1·48	7·71	1·69	5·90	1·97	20·6	2·06	19·4	1·27	5·45	<3·09	3·23	<1·54	0·60	0·15	1·59	1·38	29·5	26·9	28·1	<1·23
Sm	2·12	1·01	1·80	0·76	2·33	1·26	1·67	2·54	4·72	1·17	3·55	<1·32	1·56	<4·03	1·02	2·28	0·25	<0·10	0·83	0·96	4·21	3·81	3·97	<0·98
Eu	0·48	0·41	0·46	0·28	0·85	0·44	0·63	0·83	1·79	0·41	1·75	0·66	0·47	0·93	0·32	0·66	0·10	0·85	0·37	0·31	0·86	0·77	0·82	0·73
Gd	1·29	1·39	1·17	1·24	2·53	2·17	2·26	3·60	5·28	1·81	4·04	2·40	1·63	5·11	1·15	2·84	0·32	<0·11	1·28	0·99	1·80	1·65	1·92	<1·11
Tb	0·18	0·29	0·17	0·24	0·44	0·59	0·42	1·04	0·80	0·17	0·82	0·23	0·33	0·48	0·24	0·30	0·06	0·01	0·21	0·19	0·14	0·13	0·13	<0·01
Dy	0·71	2·10	0·74	1·61	2·60	5·11	2·71	9·32	4·84	3·98	4·05	5·82	2·39	9·68	1·68	8·77	0·64	<0·11	1·71	1·77	0·58	0·40	0·38	<0·10
Ho	0·11	0·41	0·12	0·41	0·52	1·36	0·57	3·20	0·80	1·16	0·65	1·93	0·50	3·74	0·38	2·59	0·19	<0·02	0·42	0·50	0·07	0·04	0·07	<0·06
Er	0·35	1·36	0·33	1·29	1·54	4·22	1·50	12·0	1·94	3·49	1·78	6·36	1·52	14·3	0·92	9·04	0·68	<0·07	1·31	1·80	0·12	0·07	0·09	<0·06
Tm	0·04	0·23	0·04	0·22	0·23	0·69	0·22	2·10	0·27	0·58	0·25	1·11	0·20	2·52	0·13	1·62	0·14	<0·02	0·23	0·26	<0·02	<0·02	<0·02	<0·05
Yb	0·16	1·59	0·17	1·60	1·42	4·78	1·43	15·5	1·56	3·94	1·43	8·01	1·03	18·3	0·80	11·9	0·96	<0·08	1·44	1·67	<0·11	<0·16	<0·13	<0·03
Lu	0·02	0·28	0·02	0·25	0·24	0·73	0·23	2·57	0·23	0·67	0·23	1·27	<0·11	3·15	0·12	1·74	0·18	<0·02	0·22	0·24	<0·02	<0·02	<0·02	0·02
Hf	0·66	1·14	0·68	0·95	1·30	0·66	1·03	1·04	3·41	0·53	2·43	0·73	<0·31	<1·60	<0·30	0·77	<0·10	0·14	0·21	0·14	0·38	0·42	0·50	0·10
Th	0·20	0·18	0·21	<0·32	0·46	<0·32	0·42	<0·32	0·47	0·27	0·49	<0·22	0·39	<0·46	0·35	<0·39	<0·20	26·2	<0·12	<0·09	0·03	0·04	0·05	30·7
U	0·20	0·22	0·18	<0·23	1·14	<0·21	0·37	<0·25	<0·22	0·17	<0·21	<0·24	<0·43	<0·68	<0·13	<0·33	<0·23	4·75	<0·01	<0·02	<0·02	<0·02	<0·02	4·49

Downloaded from http://petrology.oxfordjournals.org/ at University of New Orleans on June 26, 2014

Table 7: continued

Locality:	CCSD-PP1, Mesozoic UHP terrane																			
Sample:	ZMF4			ZMF6				ZMF7					ZMF8				ZML			
Mineral:	Grt	Cpx	Phl	Grt	Grt	Cpx	Cpx	Grt	Grt	Grt	Cpx	Phl	Grt	Grt	Cpx	Cpx	Cpx	Grt	Grt	Grt
Average:	5	5	3	core	rim	core	rim	core	rim	matrix	5	3	core	rim	core	rim	5	core	rim	matrix
Sc	94·8	29·1	6·56	93·0	91·1	20·5	25·5	199	113	75·9	49·5	8·38	101	92·6	21·5	25·6	19·0	100	96·3	91·0
Ti	51·0	71·7	508	84·2	70·7	36·8	83·1	199	101	49·4	70·4	331	66·5	59·8	87·8	88·0	131	909	684	339
V	150	330	38·2	108	99·0	441	353	106	67·5	90·4	324	44·6	64·4	59·7	262	305	411	139	113	117
Co	42·9	13·9	38·7	44·3	47·4	12·1	13·0	43·7	32·7	38·5	13·7	44·4	44·6	42·4	12·4	21·9	12·6	40·2	41·6	52·1
Ni	9·01	255	1286	8·14	5·40	222	251	10·5	3·77	5·66	256	1354	7·91	6·82	245	235	488	25·4	13·9	10·5
Sr	2·84	543	104	0·11	<0·161	1028	444	0·11	0·10	0·11	538	124	b.d.	0·04	151	438	340	0·04	0·10	0·06
Y	12·0	1·02	0·20	13·0	13·4	0·50	0·75	25·7	14·9	7·99	1·83	0·24	14·7	13·2	0·80	1·01	0·61	24·3	19·2	17·2
Zr	9·4	8·27	0·19	2·79	2·83	1·76	3·88	33·6	21·8	11·9	24·2	3·30	1·44	1·37	2·09	5·55	6·41	16·1	10·2	7·11
Nb	0·17	0·12	3·18	0·15	0·07	<0·03	0·06	0·10	0·07	0·04	0·07	1·11	0·13	0·08	0·05	0·09	0·04	0·06	0·06	0·07
Ba	77·7	26·5	5803	<0·23	<0·23	0·44	2·38	<0·24	<0·25	<0·18	65·4	10180	0·18	<0·19	3·13	22·7	0·39	<0·28	<0·37	<0·17
La	0·21	12·6	0·06	<0·02	<0·03	11·6	10·4	<0·01	<0·04	0·06	8·46	0·03	0·04	0·03	19·2	10·9	5·11	0·03	0·03	0·03
Ce	0·26	40·1	0·17	0·16	0·15	41·7	38·6	0·11	0·08	0·11	30·1	0·12	0·28	0·25	47·7	37·6	6·14	0·03	0·04	0·03
Pr	0·09	5·02	<0·02	0·11	0·08	6·13	5·63	0·10	0·04	0·05	4·96	<0·02	0·06	<0·02	3·37	3·86	0·54	0·02	0·02	0·02
Nd	1·14	16·9	0·31	1·04	0·85	20·5	18·8	1·10	0·79	0·94	22·1	<0·12	0·37	0·28	5·52	10·1	2·33	0·24	0·15	0·14
Sm	1·23	1·95	<0·17	0·24	<0·21	1·74	1·77	1·14	0·77	1·27	3·72	0·18	b.d.	b.d.	0·41	1·09	0·87	0·77	0·32	0·27
Eu	0·50	0·40	0·60	0·14	0·17	0·33	0·29	0·47	0·37	0·69	0·82	0·99	0·07	0·09	0·10	0·26	0·26	0·41	0·25	0·14
Gd	1·35	1·06	0·12	0·55	0·69	0·86	1·05	1·93	1·35	2·12	1·80	<0·11	0·35	0·38	0·29	0·67	0·73	1·33	1·05	0·81
Tb	0·26	0·09	<0·02	0·18	0·17	0·08	0·07	0·37	0·27	0·34	0·15	<0·02	0·14	0·13	0·04	0·09	0·08	0·42	0·32	0·29
Dy	1·85	0·38	<0·10	1·47	1·95	0·38	0·25	2·89	2·20	1·89	0·60	<0·09	1·72	1·41	0·22	0·33	0·09	3·85	2·92	2·77
Ho	0·44	0·05	<0·03	0·48	0·52	0·03	0·02	0·95	0·55	0·30	0·07	<0·02	0·57	0·48	0·03	0·05	0·02	1·00	0·74	0·69
Er	1·35	0·13	<0·12	1·49	1·48	<0·06	<0·08	4·20	2·02	0·79	0·17	<0·11	2·34	1·88	0·06	<0·08	0·04	3·52	2·36	2·55
Tm	0·22	<0·03	<0·02	0·23	0·27	<0·02	<0·02	0·81	0·34	0·11	0·02	<0·01	0·40	0·30	<0·02	<0·02	0·01	0·57	0·39	0·37
Yb	1·64	<0·13	0·09	2·00	2·07	<0·13	<0·12	7·61	2·60	0·77	0·08	<0·14	3·36	2·64	<0·13	<0·03	0·04	3·93	2·70	2·26
Lu	0·26	<0·02	<0·02	0·28	0·41	<0·02	<0·01	1·44	0·47	0·09	<0·04	<0·02	0·58	0·42	<0·02	<0·02	0·01	0·64	0·37	0·44
Hf	0·15	0·45	<0·07	<0·10	<0·12	0·21	0·15	0·46	0·24	0·23	1·14	0·11	<0·09	<0·07	<0·10	0·28	0·34	0·42	0·21	0·22
Th	0·12	0·14	11·9	<0·04	<0·05	0·04	0·08	<0·03	<0·06	0·05	0·08	29·0	<0·10	<0·02	0·29	0·10	0·07	0·03	0·07	0·09
U	0·05	0·25	3·16	<0·04	0·04	<0·02	<0·03	<0·02	<0·03	<0·05	0·03	5·49	0·07	0·06	0·04	0·04	0·03	0·07	0·06	0·04

n.a., not analysed. Data on sample ZML after Zheng *et al*. (2005*a*).

Downloaded from http://petrology.oxfordjournals.org/ at University of New Orleans on June 26, 2014

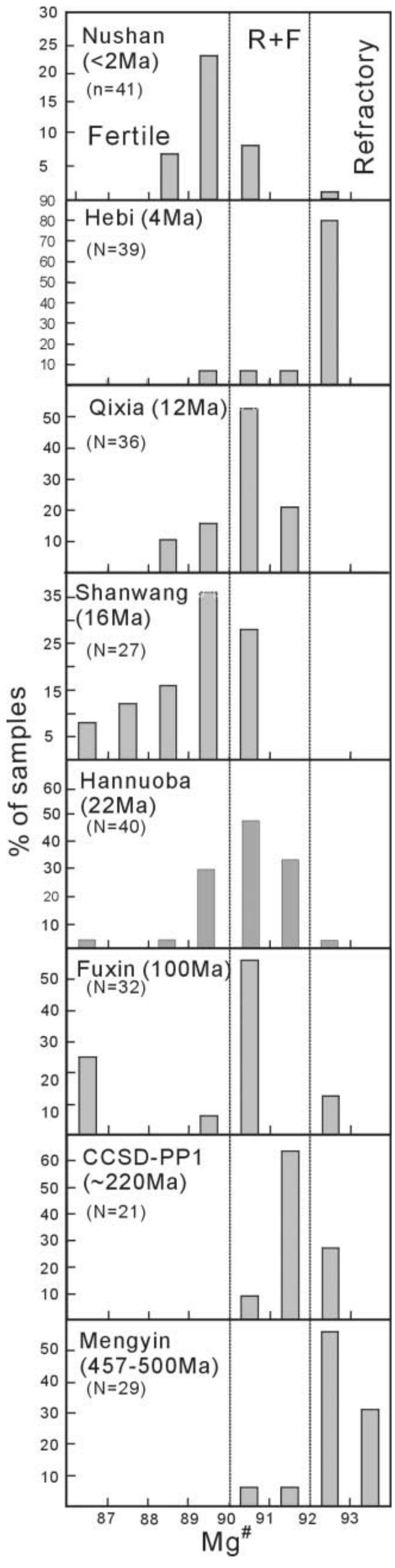

Fig. 3. Frequency distribution of Mg-number in olivine of peridotites from CCSD-PP1, Mengyin and Shanwang, and other localities. Other data sources: Mengyin, Paleozoic garnet peridotite xenoliths (Zheng, 1999; Zheng & Lu, 1999); Shanwang, Cenozoic peridotite xenoliths (Zheng *et al.*, 1998); CCSD-PP1, the UHP garnet peridotite terrane (Yang & Jahn, 2000; Zhang *et al.*, 2000, 2003; Zheng *et al.*, 2005*a*); Nushan, Cenozoic peridotite xenoliths (Xu *et al.*, 1998); Hebi, Cenozoic peridotite xenoliths (Zheng *et al.*, 2001); Qixia, Cenozoic peridotite xenoliths (Zheng *et al.*, 1998; Gao *et al.*, 2002); Hannuoba, Cenozoic peridotite xenoliths (Chen *et al.*, 2001; Gao *et al.*, 2002; Rudnick *et al.*, 2004; Yu *et al.*, 2006); Fuxin, Late Mesozoic peridotite xenoliths (Zheng *et al.*, 2006*a*). 'Refractory' and 'Fertile' peridotites are characterized by Mg-number values of olivine >92 and <90, respectively. 'R + F' represents transitional samples with olivine Mg-number between 92 and 90.

lherzolites with high CaO and Al_2O_3 contents (Zheng *et al.*, 1998). As shown in Fig. 9, all the Mengyin peridotites plot within the Archon field (Griffin *et al.*, 1999*a*). However, the bulk compositions of Shanwang peridotites fall mainly into the Tecton field, suggesting that they represent recently formed, weakly depleted lithospheric mantle (Zheng *et al.*, 1998, 2005).

Different peridotites from UHP terranes have been interpreted as having both mantle and crustal protoliths (Brueckner & Medaris, 2000; Zhang *et al.*, 2000). These peridotites may have originated (1) by UHP metamorphism of crustal ultramafic rocks during continental subduction, (2) as high P/T relict peridotites derived from ancient depleted mantle, or (3) as low P/T peridotites related to upwelling asthenosphere (Medaris, 1999). Crustal peridotites and pyroxenites are interpreted as portions of mafic–ultramafic igneous complexes formed from magmas that were intruded into the continental crust prior to subduction. They show cumulate structures and low Mg-number olivine (Zhang *et al.*, 1995). The high Mg-number olivine in the CCSD-pp1 peridotites (Table 2 and Fig. 3) makes it improbable that they represent crustal ultramafic rocks.

Although the CCSD-PP1 peridotites have low Mg-number and Cr-number (Figs 6 and 10a) in garnet, and slightly lower Mg-number in olivine (Fig. 3) compared with the Paleozoic xenoliths or xenocrysts, they have similar Cr-number, Mg-number, and minor elements (e.g. Na_2O, Al_2O_3 and TiO_2) in diopside (Fig. 4), and similar HREE and Y in garnet (especially in garnet cores; Fig. 10b–d). The UHP peridotites also have similar whole-rock Mg-number and Mg/Si (Fig. 9) to the Paleozoic xenoliths, indicating that the CCSD-PP1 samples represent a refractory mantle protolith that experienced re-equilibration under relatively low-T conditions, producing magnesium-rich phlogopite (e.g. mean 18 Mg/Fe) and more Fe-rich garnet and less magnesian olivine. The differences in olivine composition between the CCSD-PP1 peridotites and the Mengyin and Hebi xenoliths (Fig. 3), therefore, are consistent with an overall bulk composition for the CCSD-PP1 peridotites that is less depleted than

Downloaded from http://petrology.oxfordjournals.org/ at University of New Orleans on June 26, 2014

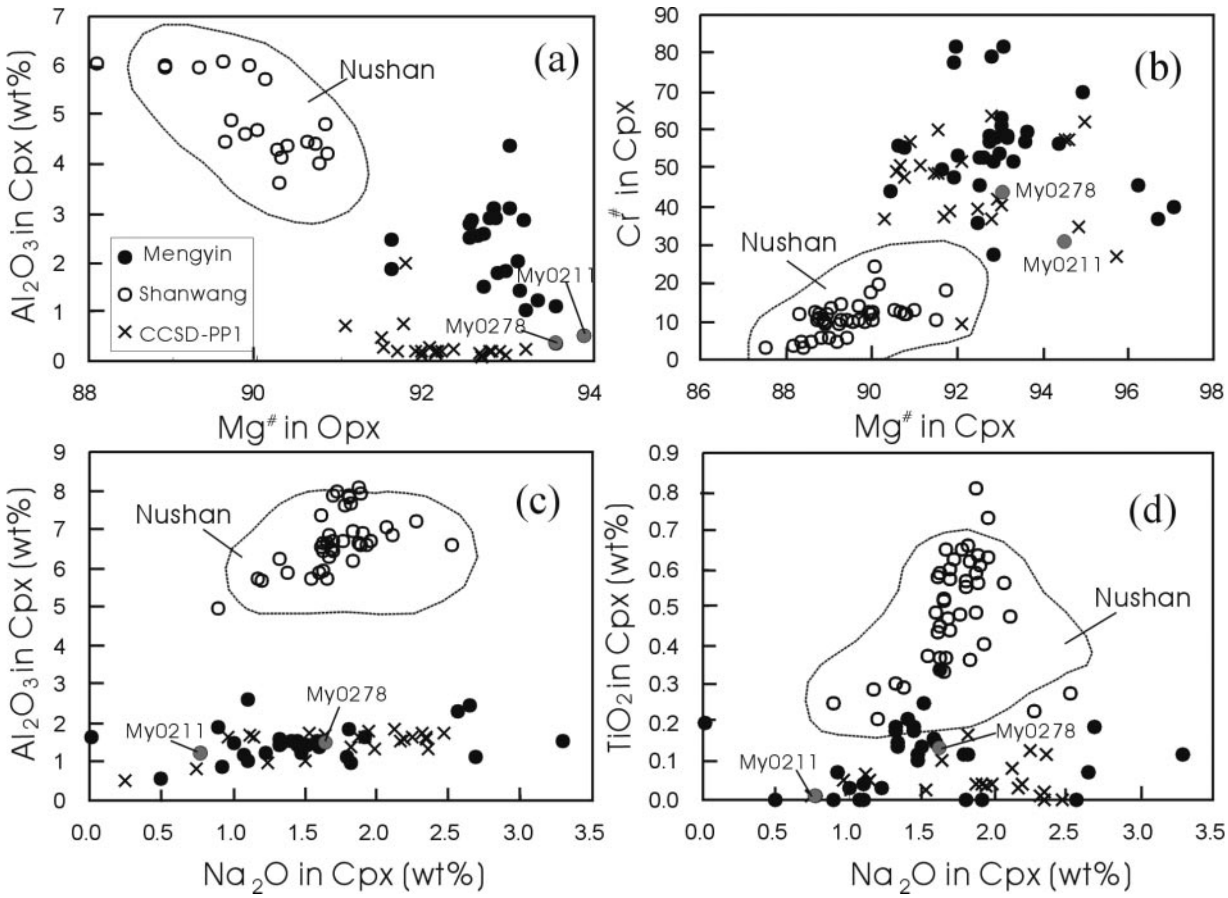

Fig. 4. (a) Mg-number in Opx vs Al_2O_3 in Cpx; (b) Mg-number vs Cr-number in Cpx; (c) Na_2O vs Al_2O_3 in Cpx; (d) Na_2O vs TiO_2 in Cpx. The Nushan field encloses analyses of pyroxenes from peridotite xenoliths in the Cenozoic Nushan basalts (Xu *et al.*, 1998, 2000; $n = 41$). Other data sources as in Fig. 3.

the Archean lithospheric mantle, but more depleted than the Cenozoic xenoliths.

Metasomatism recorded in peridotitic diopsides

Enrichment of large ion lithophile elements (LILE) and LREE in mantle diopside has been attributed to metasomatism by carbonatitic melts (e.g. Meen, 1987; Yaxley *et al.*, 1991, 1998), volatile-rich silicate melts (Zangana *et al.*, 1999) or H_2O–CO_2 fluids (Ionov *et al.*, 1997; Stalder *et al.*, 1998). All of these different fluid types may coexist in space and time, as a result of chromatographic fractionation processes during melt intrusion in the upper mantle (e.g. Bodinier *et al.*, 2004). Trace-elemental partitioning between diopside and melt has been experimentally determined for carbonate and silicate systems at mantle conditions (Blundy & Dalton, 2000). The results show that diopside–melt partition coefficients for Si, Al, HREE, Ti and Zr in the carbonate system are higher by factors of 5–200 than in the silicate system. Partition coefficients for Nb, LREE and alkali metals show much less fractionation (<3 times; Blundy & Dalton, 2000). On the other hand, relative to silicate melt or CO_2-rich fluid, carbonatite melts can fractionate REE and high field strength elements (HFSE) more effectively (Blusztajn & Shimizu, 1994) and have high contents of LILE (Meen, 1987). High HFSE depletion and low Ti/Eu ratios in mantle diopside, coupled with LREE enrichment, have been widely interpreted as the key signatures of carbonatite-related metasomatism (e.g. Klemme *et al.*, 1995; Yaxley *et al.*, 1998; Coltorti *et al.*, 1999).

Metasomatic signatures in the peridotitic diopsides studied here include: (1) enrichment in Th, U, Sr, LREE, and (2) fractionation of Zr, Ti and Nb from the LREE (Fig. 5). The diopsides in the Cenozoic (Shanwang) xenoliths have low $(La/Yb)_n$ (<20) and wide ranges of Ti/Eu (1400–4500), suggesting 'silicate metasomatism'. In contrast, diopsides in both the Mengyin xenoliths and the CCSD-PP1 peridotites have high $(La/Yb)_n$ (>20) and low Ti/Eu (<1500), suggesting

Downloaded from http://petrology.oxfordjournals.org/ at University of New Orleans on June 26, 2014

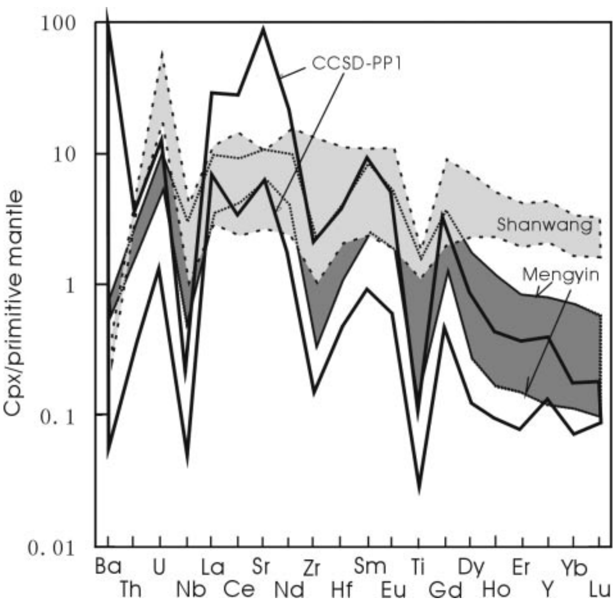

Fig. 5. Primitive mantle-normalized (McDonough & Sun, 1995) trace element patterns of clinopyroxenes from Mengyin, Shanwang and CCSD-PP1. Mengyin data include both clinopyroxenes from xenoliths, and xenocrysts from heavy-mineral concentrates.

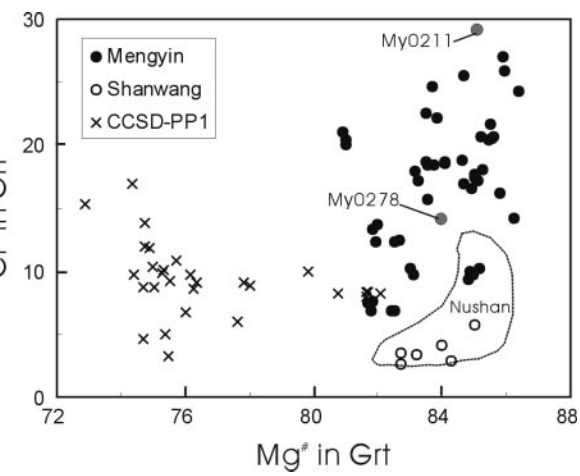

Fig. 6. Mg-number vs Cr-number in garnets from Mengyin, Shanwang and CCSD-PP1. Nushan field encloses garnets from spinel–garnet peridotite xenoliths in Cenozoic Nushan basalts (Xu *et al.*, 1998, 2000; $n = 11$).

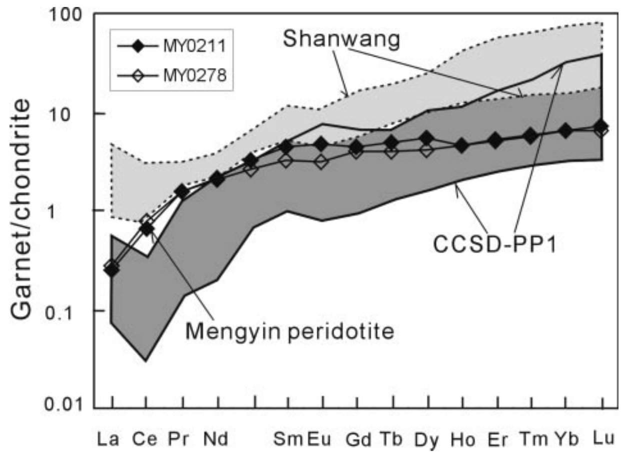

Fig. 7. Representative REE patterns of garnets from the CCSD-PP1, Shanwang and Mengyin (xenoliths and xenocrysts) peridotites.

'carbonatitic' metasomatism (Fig. 11). Although these data might suggest that carbonatite-style metasomatism was more prominent in the thicker, older lithosphere, it should be noted that both types of metasomatism have been described in xenoliths from other Cenozoic localities (e.g. Xu *et al.*, 2000). The Hf-isotope and trace-element compositions of zircons in the CCSD-PP1 peridotites also suggest that the peridotitic body underwent metasomatism by kimberlititic and/or carbonatitic agents derived from ~1·4 Ga (T_{DM}) asthenospheric mantle (Zheng *et al.*, 2006*b*). Therefore, we consider that the CCSD-PP1 peridotites represent cratonic mantle protoliths that have interacted with mantle-derived melts or fluids in Mesoproterozoic time and experienced subsolidus re-equilibration involving fluids/melts derived from the subducted continental crust (phlogopite-forming) during UHP metamorphism in the early Mesozoic.

Late Mesozoic–Cenozoic mantle replacement

The xenoliths entrained in the Cenozoic basalts of the North China Craton are generally much less depleted than those found in the Paleozoic kimberlites, which were derived from a thick cratonic lithosphere (Fig. 12a). This suggests that the Cenozoic lithospheric mantle consists largely of newly accreted materials; these now constitute much of the SCLM beneath the eastern North China Craton (Griffin *et al.*, 1998*b*; Fan *et al.*, 2001; Gao *et al.*, 2002) especially in areas near the translithospheric Tanlu fault (Zheng *et al.*, 1998; Xu *et al.*, 2000). Less common, more depleted xenoliths in areas far from the Tanlu fault (e.g. in Hebi; Zheng *et al.*, 2001) may represent relics of the Archean lithosphere, preserved locally at relatively shallow levels. Archean SCLM is dificult to remove by tectonic processes, being buoyant and refractory (Poudjom Djomani *et al.*, 2001). Therefore, extension and/or erosion of the lithosphere may be the most likely mechanism for the modification of the ancient lithospheric keel (Griffin *et al.*, 1998*b*; Zheng *et al.*, 1998; Zheng, 1999; Fan *et al.*, 2001; Xu, 2001).

Most of the mantle-derived Sulu UHP garnet peridotites along the southern margin of the North China Craton are more depleted than the xenoliths in Cenozoic basalts (except for Hebi; see Fig. 3). They also have more radiogenic Sr and less radiogenic Nd

Downloaded from http://petrology.oxfordjournals.org/ at University of New Orleans on June 26, 2014

Table 8: P–T estimates for the garnet peridotites

Sample		R96 Ni in Grt T (°C)	KR00 Cpx–Grt T (°C)	ONW79 Opx–Grt T (°C)	BK90 T (°C)	BK90 Grt–Opx P (kbar)
Mengyin, Paleozoic						
MY0211		1145	1012	1097	1093	59·7
MY0278		1196	1136	1087	1112	55·9
Shanwang, Cenozoic						
SW0169		1175	1119	1340	1002	17·0
SW0193		1193	1278	1457	1101	19·9
SW01-1		1173	1243	1333	1160	22·6
SW01-8		1190	1263	1378	1179	24·0
SW04-2		1157	1066	1351	1087	16·2
SW04-6		1215	1242	1461	1172	19·6
CCSD-PP1, Mesozoic						
ZMF2		559				
ZMF3	Cores	662	715	605	688	37·4
	Rims	569	718	621	684	36·1
ZMF4		644	745	617	716	45·3
ZMF6	Cores	628	865	776	729	42·7
	Rims	569	800	770	730	43·0
	Matrix		701	595	687	30·8
ZMF7	Cores	670	931	962	772	54·0
	Rims	524	712	645	763	51·6
	Matrix	576	725	645	766	52·5
ZMF8	Cores	624	833	716	707	42·7
	Rims	602	790	663	710	43·5
ZML	Cores	845	1108	954	678	38·4
	Rims	718	916	665	672	36·5
	Matrix	669	834	603	659	32·6

R96, temperatures are estimated by using the method of Ryan *et al*. (1996); others are given for mineral pairs after the methods of KR00 (Krogh Ravna , 2000), ONW79 (O'Neill & Wood, 1979) and BK90 (Brey & Kohler, 1990). Data on sample ZML after Zheng *et al*. (2005*a*).

isotopic compositions than depleted mantle (Yang & Jahn, 2000; Zhang *et al*., 2000), and thus are similar to the peridotites from the Paleozoic kimberlites (Zheng, 1999), representing ancient depleted lithospheric mantle. These similarities in bulk and isotopic composition suggest that the Sulu peridotites are derived from the subcontinental lithospheric mantle (Figs 4 and 9–11). The early Mesozoic northward subduction (Fig. 12b) of the Yangtze Craton beneath the southern margin of the North China Craton would have resulted in metasomatism by fluids and/or melts derived from the subducted continental crust (on the lower part of the North China Craton) and the lateral spreading of the upper part of the continental lithospheric mantle of the North China Craton (Fig. 12c). The early Mesozoic

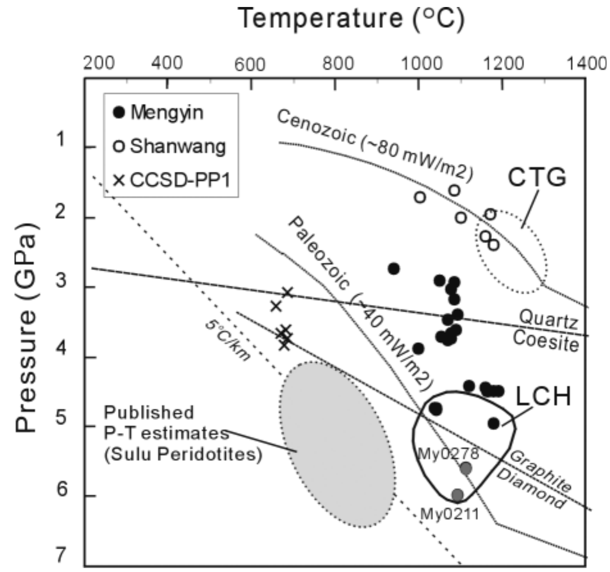

Fig. 8. Pressures and temperatures, estimated using methods of Brey & Kohler (1990), for Paleozoic, Mesozoic and Cenozoic lithosphere (see Table 8). T_{Ni}–P_{Cr} estimates (Ryan *et al*., 1996) are shown for xenocrystic garnets from the Mengyin kimberlites (this work) and lherzolitic garnets from Cenozoic basalts, eastern China (CTG; Y. G. Xu *et al*., 1995; X. Xu *et al*., 1998, 2000). Paleozoic and Cenozoic geotherms are after Lu & Zheng (1996) and Griffin *et al*. (1998*a*); LCH, field of T_{Ni}–P_{Cr} estimates for xenocrystic low-Ca harzburgite garnets from Mengyin kimberlites (GEMOC unpublished database). Published *P–T* estimates for the Sulu perdotites are after Yang *et al*. (1993), Zhang *et al*. (1995, 2000, 2003) and Yang & Jahn (2000). Graphite–diamond and quartz–coesite transitions are from Kennedy & Kennedy (1976) and Bohlen & Boettcher (1982), respectively.

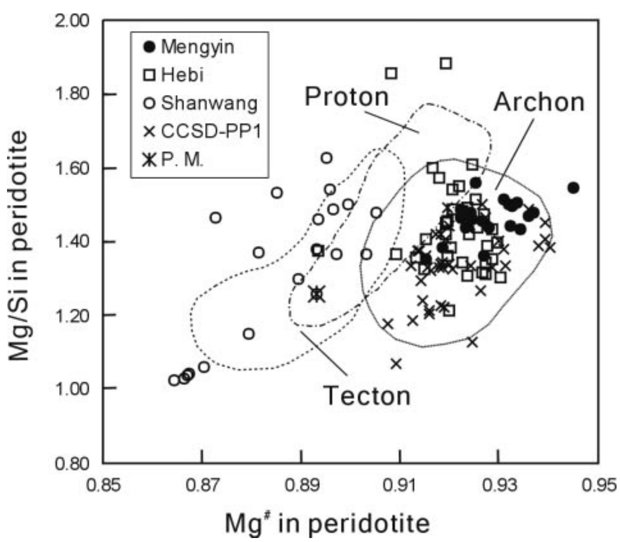

Fig. 9. Mg-number vs Mg/Si of peridotites for Paleozoic, Mesozoic and Cenozoic lithosphere. Archon (>2·5 Ga), Proton (2·5–1·0 Ga) and Tecton (<1·0 Ga) fields are from Griffin *et al*. (1999*a*); Mengyin, Zheng & Lu (1999) and Zheng (1999); Shanwang (newly accreted lithospheric mantle), Zheng *et al*. (1998); CCSD-PP1, Li *et al*. (2003); Hebi (shallow relics of Archean cratonic mantle), Zheng *et al*. (2001). P.M., Primitive mantle (McDonough & Sun, 1995).

Downloaded from http://petrology.oxfordjournals.org/ at University of New Orleans on June 26, 2014

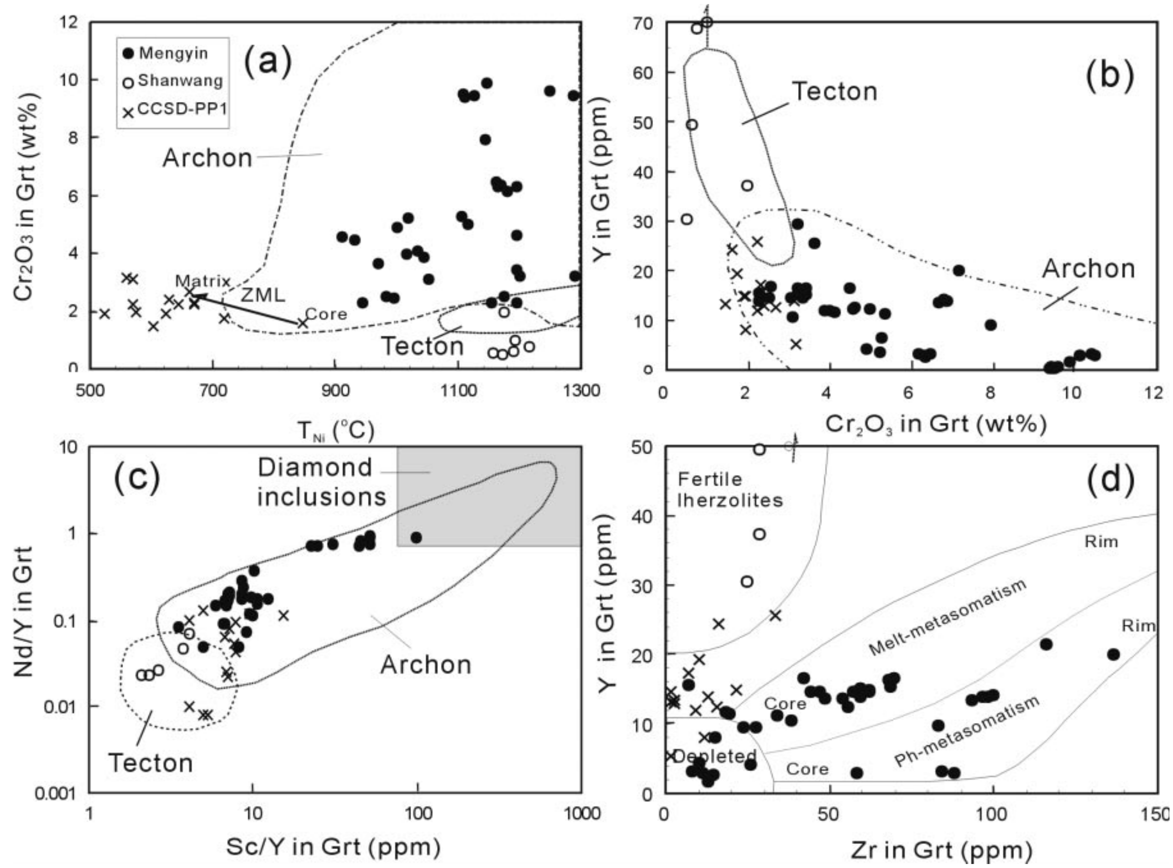

Fig. 10. Cr_2O_3 in garnet vs T_{Ni} (a); Cr_2O_3 vs Y in garnet; (c) Nd/Y vs Sc/Y in garnet; (d) Zr vs Y in garnet. Fields for diamond-inclusion garnets, and garnets from Archon and Tecton, after Griffin *et al.* (1998*a*, 1998*b*, 1999*a*, 1999*b*). Fields showing trace-element signatures of garnets from depleted harzburgite and fertile lherzolite, and different metasomatic styles are from Griffin & Ryan (1995). Melt-related metasomatism is typical of high-*T* sheared lherzolite xenoliths in kimberlites; phlogopite-related metasomatism is seen in garnets from shallower phlogopite-rich lherzolites in kimberlites. Core–rim zoning with increase in Zr is characteristic of both metasomatic styles (Griffin & Ryan, 1995). Data for sample ZML from Zheng *et al.* (2005*a*).

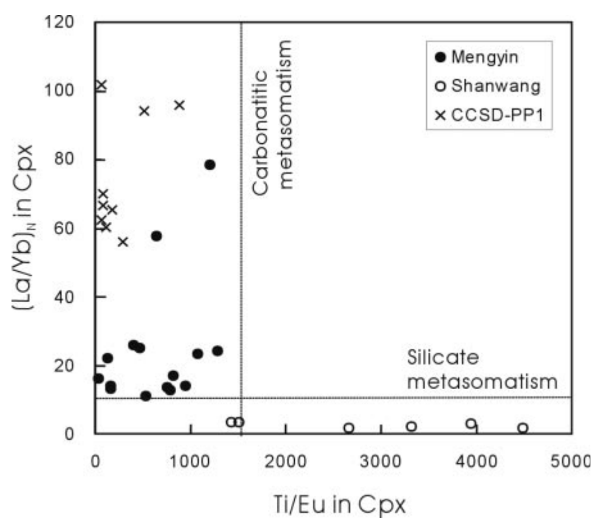

Fig. 11. Ti/Eu vs $(La/Yb)_N$ (chondrite-normalized) of Cpx in the CCSD-PP1, Mengyin and Shanwang peridotites. Signatures of silicate and carbonatitic metasomatism are modified after Coltorti *et al.* (1999).

Xinyang basalts (Fig. 12d) and the late Mesozoic (early Cretaceous) basaltic rocks from the southern margin of the North China Craton are characterized by enrichment in LILE and LREE but depletion in HFSE and have EM1-like Sr–Nd isotopic compositions. They are interpreted as having originated from a Paleozoic mantle source that had undergone extensive interaction with a subducted crustally derived melt (H. F. Zhang *et al.*, 2002, 2003; Guo *et al.*, 2003; Zheng *et al.*, 2005*b*).

The sedimentary basins of eastern China were formed in two episodes, one in the Jurassic–Cretaceous and the second in the Eocene (Li *et al.*, 1997). These periods coincide with two peaks of heat flow calculated from coal reflectivity (R_o) measurements in the Songliao Basin: 99 mW/m^2 at 115 Ma and 87 mW/m^2 at 57 Ma (Li, 1995). However, it should be noted that the Songliao Basin lies about 800–1000 km NE of the study areas, so similarities in tectonism at this time assume that the northeastern region of China was affected by similar and cotemporaneous tectonic events. These thermal episodes

Downloaded from http://petrology.oxfordjournals.org/ at University of New Orleans on June 26, 2014

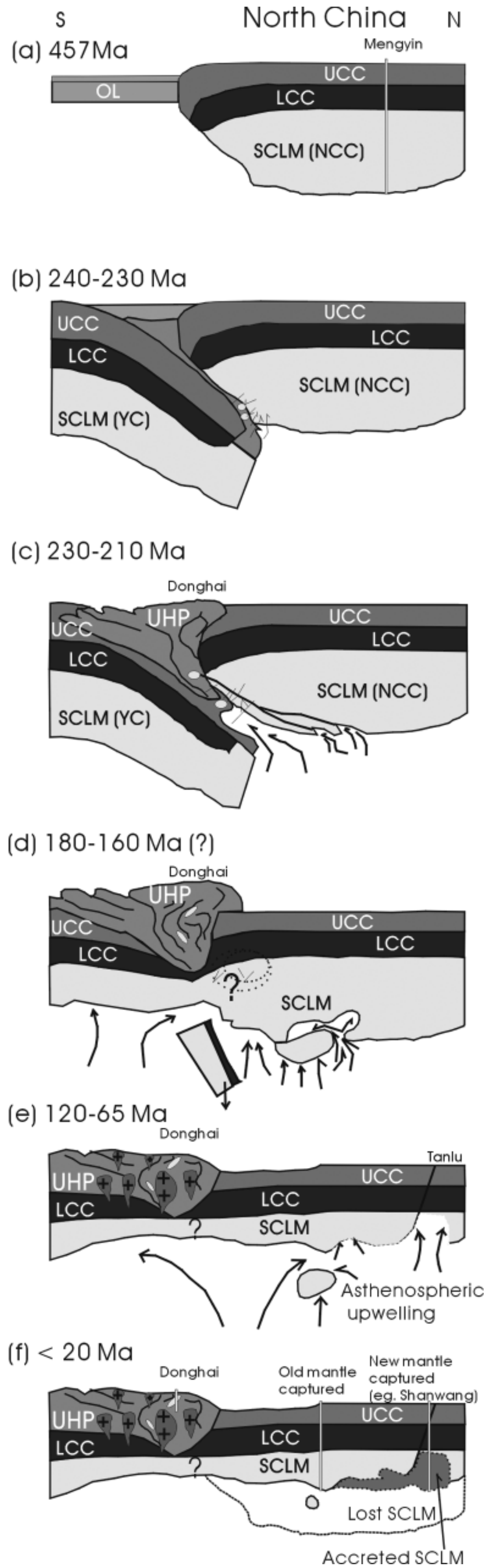

may have accompanied asthenospheric upwelling, and may be related to subduction of the Kula Plate in Jurassic–Cretaceous time and the Pacific Plate in the Tertiary (Ma *et al.*, 1984; Menzies *et al.*, 1993; Griffin *et al.*, 1998*a*). Thus, the Jurassic–Cretaceous and Eocene could be the most important time periods in the modification of the lithospheric mantle. Seismic tomography data (Sun, 1992; Yuan, 1996) suggest that lower-velocity material in the upper mantle welled up along the translithospheric fault (Fig. 12e) from depths >150 km, and flowed along weak zones in the mantle at about 60–130 km depth, forming a 'mushroom-cloud' structure beneath the eastern part of the North China Craton near 36°N (Lu & Zheng, 1996; Yuan, 1996; Lu *et al.*, 2000). The newly accreted lithospheric mantle, represented by the xenoliths in late Mesozoic (~100 Ma) Fuxin basalts and most of the Neogene basalts (e.g. Shanwang, Nushan), is fertile (see Fig. 3) but has depleted Sr–Nd isotopic compositions (Zheng, 1999; Fan *et al.*, 2001). It is interpreted as cooled asthenosphere (O'Reilly *et al.*, 2001; Zheng *et al.*, 2005*c*), which welled up at least 100 Myr ago based on the occurrence of fertile xenoliths in Fuxin basalts; cooling of this material would deepen the boundary between the lithosphere and asthenosphere (Fig. 12f). Therefore, lateral spreading of lithosphere and asthenospheric erosion is the most possible mechanism for the lithospheric thinning. Meanwhile, the cooling of the welled asthenosphere would result in a little of lithospheric thickening and achieve the replacement of the old refractory lithosphere by the newly accreted fertile mantle.

In summary, the three types of garnet peridotites that form the basis of this study are derived from Paleozoic,

Fig. 12. Schematic illustration of a model for lithospheric mantle evolution in eastern China. (a) Early Paleozoic (~463 Ma): Mengyin kimberlites are generated from the base of a thick cratonic lithosphere with a low geotherm (~40 mW/m^2); (b) 240–230 Ma: subduction of the edge of the Yangtze Craton results in the emplacement of solid fragments of the lithospheric mantle of the North China Craton in the top of the crustal slab; (c) 230–210 Ma: the lithospheric mantle splits apart from the North China Craton during the collision and exhumation at ~210 Ma; (d) 180–160 Ma(?): progressive exhumation of the UHP rocks of the Sulu terrane raises the peridotite body from mantle to shallow crustal depths, triggered by the detachment of the subducted slab; (e) 120–65 Ma: asthenospheric upwelling, possibly related to subduction of the Kula Plate in Late Jurassic–Cretaceous time and the Pacific Plate in the Tertiary, erodes the remaining lithospheric mantle including those newly accreted lithosphere derived from the early cooling of the welled asthenosphere at ~100 Ma (Zheng *et al.*, 2006*a*); (f) <20 Ma: progressing asthenospheric cooling lowers the boundary between the lithosphere and the asthenosphere and creates newer lithospheric mantle, derived from the upwelling asthenosphere in the Tertiary; eruption of Cenozoic alkali basalts. Therefore, a fluctuant boundary between lithosphere and asthenosphere derived from their secular interaction (asthenospheric upwelling and cooling). SCLM, subcontinental lithospheric mantle; UCC, upper continental crust; LCC, lower continental crust; OL, oceanic lithosphere; UHP, ultrahigh-pressure rocks; NCC, North China Craton; YC, Yangtze Craton.

Downloaded from http://petrology.oxfordjournals.org/ at University of New Orleans on June 26, 2014

Mesozoic and Cenozoic subcontinental lithospheric mantle (SCLM) in eastern China: (1) refractory but partly refertilized SCLM in the Paleozoic kimberlite xenoliths; (2) metasomatized mantle in the Sulu peridotites, which must originally have been rather similar to the Paleozoic xenoliths; (3) newly accreted fertile lithospheric mantle derived from the cooling of the upwelling asthenosphere, represented by xenoliths in Cenozoic basalts.

CONCLUSIONS

(1) Geochemical criteria establish three distinct origins for mantle-derived garnet peridotites in eastern China. Garnet peridotites in Paleozoic kimberlites represent Archean lithospheric mantle, refertilized to varying extents. Mantle-derived peridotites in the Sulu ultrahigh-pressure terrane represent less strongly depleted SCLM domains, of at least Proterozoic age. Garnet peridotite xenoliths in Cenozoic basalts represent newly accreted lithospheric mantle derived by small degrees of partial melting of asthenospheric mantle.

(2) The mantle-derived peridotites from the Sulu ultrahigh-pressure (UHP) terrane show strong similarities to the old depleted mantle in the North China Craton, sampled by Paleozoic kimberlites. The relatively small differences in degree of depletion can be attributed to subsequent (probably Proterozoic) metasomatic overprints, whereas differences in mineral chemistry reflect both bulk-compositional differences and re-equilibration during ultrahigh-pressure metamorphism in the early Mesozoic.

(3) The detailed comparisons of geochemical differences between the lithospheric mantle sampled as xenoliths in Paleozoic kimberlites and late Tertiary basalts within the North China Craton reinforce previous studies suggesting that there was a dramatic change in the composition, thermal state and thickness of the SCLM. This change probably reflects extension and disruption of the old buoyant refractory lithospheric keel, related to the Mesozoic continental subduction that produced the Dabie–Sulu ultrahigh-pressure terrane.

ACKNOWLEDGEMENTS

The authors would like to thank Dr Norman Pearson and Ms Suzy Elhou for invaluable guidance and assistance with the analytical work at GEMOC. Chinese NSF (40521001 and 40425002) and '973' projects (2003CB716500), and ARC Discovery Project and Linkage International grants (to S.Y.O'R. and W.L.G.) supported this study. Analytical data reported here were collected using instrementation purchased with funding from DEST Infrastructure, ARC LIEF, and Macquarie University funds. This is Contribution 438 from the ARC National Key Centre for the Geochemical Evolution and Metallogeny of Continents (GEMOC). We thank L. Morten, T. Hirajima, M. Menzies and M. Wilson for constructive reviews and suggestions.

REFERENCES

Bernstein, S., Kelemen, P. B. & Brooks, C. K. (1998). Depleted spinel harzburgite xenoliths in Tertiary dykes from East Greenland: restites from high degree melting. *Earth and Planetary Science Letters* **154**, 221–235.

Blundy, J. & Dalton, J. (2000). Experimental comparison of trace element partitioning between clinopyroxene and melt in carbonate and silicate systems, and implications for mantle metasomatism. *Contributions to Mineralogy and Petrology* **139**, 356–371.

Blusztajn, J. & Shimizu, N. (1994). The trace-element variations in clinopyroxenes from spinel peridotite xenoliths from southwest Poland. *Chemical Geology* **111**, 227–243.

Bodinier, J. L., Menzies, M. A., Shimizu, N., Frey, F. A. & McPherson, E. (2004). Hydrous, silicate and carbonate metasomatism at Lherz, France: contemporaneous derivatives of silicate melt–harzburgite reaction. *Journal of Petrology* **45**, 299–320.

Bohlen, S. R. & Boettcher, A. L. (1982). The quartz–coesite transformation: a precise determination and the effects of other components. *Journal of Geophysical Research* **87**, 7073–7078.

Boyd, F. R. (1996). Origin of peridotite xenoliths: major element consideration. In: Ranalli, G., Ricci Lucchi, F., Ricci, C. A. & Trommosdorff, T. (eds) *High Pressure and High Temperature Research on Lithosphere and Mantle Materials*. Siena: University of Siena, pp. 89–106.

Brey, G. P. & Kohler, T. (1990). Geothermobarometry in four-phase lherzolites I: experimental results from 10 to 60 kb. *Journal of Petrology* **31**, 1313–1352.

Brueckner, H. K. & Medaris, L. G. (2000). A general model for the intrusion and evolution of mantle garnet peridotites in high-pressure and ultra-high pressure metamorphic terranes. *Journal of Metamorphic Geology* **18**, 123–134.

Carswell, D. A., Wilson, R. N. & Zhai, M. (2000). Metamorphic evolution, mineral chemistry and thermobarometry of schists and orthogeneisses hosting ultra-high pressure eclogites in Dabieshan of central China. *Lithos* **52**, 121–155.

Chen, S. H., O'Reilly, S. Y., Zhou, X. H., Griffin, W. L., Zhang, G. H., Sun, M., Feng, J. L. & Zhang, M. (2001). Thermal and petrological structure of the lithosphere beneath Hannuoba, Sino-Korean craton, China: evidence from xenoliths. *Lithos* **56**, 267–301.

Chi, J. S., Lu, F. X., Zhao, L., Zhao, C. H. & Zheng, J. P. (1996). *Kimberlites and Paleozoic Mantle beneath North China Platform*. Beijing: Science Press, 292pp. (in Chinese).

Coltorti, M., Bonadiman, C., Hinton, R. W., Siena, F. & Upton, B. G. (1999). Carbonatite metasomatism of the oceanic upper mantle: evidence from clinopyroxenes and glasses in ultramafic xenoliths of Grande Comore, Indian Ocean. *Journal of Petrology* **40**, 133–165.

Ernst, W. G. (1988). Element partitioning and thermobarometry in polymetamorphic late Archean and Early–Mid Proterozoic rocks from eastern Liaoning and southern Jilin Provinces, China. *American Journal of Science* **288A**, 293–340.

Fan, Q. C. & Hooper, P. R. (1989). The mineral chemistry of ultramafic xenoliths of Eastern China: implications for upper mantle composition and the paleogeotherms. *Journal of Petrology* **30**, 1117–1158.

Downloaded from http://petrology.oxfordjournals.org/ at University of New Orleans on June 26, 2014

Fan, W. M., Zhang, H. F., Baker, J., Jarvis, K. E., Mason, P. R. D. & Menzies, M. A. (2001). On and off the North China craton: where is the Archean keel? *Journal of Petrology* **41**, 933–950.

Gao, S., Rudnick, R. L., Carlson, R. W., McDonough, W. F. & Liu, Y. S. (2002). Re–Os evidence for replacement of ancient mantle lithosphere beneath the North China craton. *Earth and Planetary Science Letters* **198**, 307–322.

Gaul, O. F., Griffin, W. L., O'Reilly, S. Y. & Pearson, N. J. (2000). Mapping olivine composition in the lithospheric mantle. *Earth and Planetary Science Letters* **182**, 223–235.

Griffin, W. L. & Ryan, C. G. (1995). Trace elements in indicator minerals: area selection and target evaluation in diamond exploration. *Journal of Geochemical Explorations* **53**, 311–337.

Griffin, W. L., O'Reilly, S. Y. & Ryan, C. G. (1992). Composition and thermal structure of the lithosphere beneath South Africa, Siberia and China: proton microprobe studies. *International Symposium on Cenozoic Volcanic Rocks and Deep-seated Xenoliths of China and its Environs. Beijing,* 20 pp.

Griffin, W. L, Zhang, A. D., O'Reilly, S. Y. & Ryan, C. G. (1998a). Phanerozoic evolution of the lithosphere beneath the Sino-Korean craton. In: Flower, M., Chung, S. L., Lo, C. H. & Lee, Y. Y. (eds) *Mantle Dynamics and Plate Interactions in East Asia. American Geophysical Union, Geodynamics Series* **27**, 107–126.

Griffin, W. L., O'Reilly, S. Y., Ryan, C. G., Gaul, O. & Ionov, D. I. (1998b). Secular variation in the composition of subcontinental lithospheric mantle: geophysical and geodynamic implications. In: Braun, J., Dooley, J. C., Goleby, B. R., van der Hilst, R. D. & Klootwijk, C. T. (eds) *Structure and Evolution of the Australian Continent. American Geophysical Union, Geodynamics Series* **26**, 1–26.

Griffin, W. L., Fisher, N. I., Friedman, J., Ryan, C. G. & O'Reilly, S. Y. (1999a). Cr-pyrope garnets in the lithospheric mantle. I. Compositional systematics and relationships to tectonic setting. *Journal of Petrology* **40**, 679–704.

Griffin, W. L., O'Reilly, S. Y. & Ryan, C. G. (1999b). The composition and origin of sub-continental lithospheric mantle. In: Fei, Y., Berka, C. M. & Mysen, B. O. (eds) *Mantle Petrology: Field Observations and High-pressure Experimentation: a Tribute to Francis R. (Joe) Boyd. Geochemical Society, Special Publications* **6**, 13–45.

Guo, F., Fan, W., Wang, Y. & Lin, G. (2003). Geochemistry of late Mesozoic mafic magmatism in west Shandong Province, eastern China: characterizing the lost lithospheric mantle beneath the North China Block. *Geochemical Journal* **37**, 63–77.

Hart, S. R. & Zindler, A. (1986). In search of bulk Earth composition. *Chemical Geology* **57**, 247–267.

Harte, B. (1977). Chemical variations in upper mantle nodules from southern African kimberlites. *Journal of Petrology* **85**, 279–288.

He, G. P., Ye, H. W. & Ye, H. W. (1992). The evolution and metamorphism of Jidong high-pressure granulites. *Acta Petrologica Sinica* **8**, 128–135 (in Chinese).

Hirajima, T. & Nakamura, D. (2003). The Dabie Shan–Sulu orogen. In: Carswell, D. A. & Compagnoni, R. (eds) *Ultrahigh Pressure Metamorphism. European Mineralogical Union, Notes in Mineralogy* **5**, 105–144.

Hirajima, T., Ishiwatari, A, Cong, B., Zhang, R. Y., Banno, S. & Nozaka, T. (1990). Identification of coesite in Mengzhong eclogite from Donghai county, northeastern Jiangsu Province, China. *Mineralogy Magazine* **54**, 578–584.

Ionov, D. A., O'Reilly, S. Y. & Griffin, W. L. (1997). Volatile-bearing minerals and lithophile trace elements in the upper mantle. *Chemical Geology* **141**, 153–184.

Jahn, B. M. (1990). Origin of high-pressure granulites: geochemical constraints form Archean high-pressure granulite facies rocks of the Sino-Korean craton, China. In: Vielzeuf, D. & Vidal, Ph. (eds) *High-pressure Granulites and Crustal Evolution. NATO ASI Series, Series C: Mathematical and Physical Sciences* **311**, 471–492.

Jahn, B. M. (1998). Geochemical and isotopic characteristics of UHP eclogites and ultramafic rocks of the Dabie orogen: implications for continental subduction and collisional tectonics. In: Hacker, B. R. & Liou, J. G. (eds) *When Continental Collide: Geodynamics and Geochemistry of Ultrahigh-Pressure Rocks*. Dordrecht: Kluwer Academic, pp. 203–239.

Jin, L. Y. (1985). Xenoliths in Cenozoic basalts from Tanlu fault. *Journal of Changchung College of Geology* **3**, 21–32, (in Chinese).

Kennedy, C. A. & Kennedy, G. C. (1976). The equilibrium boundary between graphite and diamond. *Journal of Geophysical Research* **81**, 2467–2470.

Klemme, S., van der Laan, S. R., Foley, S. F. & Gunther, D. (1995). Experimentally determined trace and minor element partitioning between clinopyroxene and carbonatite melt under upper mantle conditions. *Earth and Planetary Science Letters* **133**, 439–448.

Krogh Ravna, E. (2000). The garnet-clinopyroxene Fe^{2+}–Mg geothermometer: an update calibration. *Journal of Metamorphic Geology* **18**, 211–219.

Le Maitre, R. W. (1982). *A Classification of Igneous Rocks and Glossary of Terms*. Oxford: Blackwell Scientific.

Li, S. G., Xiao, Y., Liou, D., Chen, Y., Ge, N., Zhang, Z., Sun, S., Cong, B., Zhang, R., Hart, S. R. & Wang, S. (1993). Collision of the North China and Yangtze Blocks and formation of coesite-bearing eclogites: timing and processes. *Chemical Geology* **109**, 89–111.

Li, S. T., Lu, F. X. & Lin, C. S. (1997). *Evolution of Mesozoic and Cenozoic Basins in Eastern China and their Dynamic Background*. Wuhan: China University of Geosciences, 237 pp. (in Chinese).

Li, T. F., Yang, J. S. & Zhang, R. Y. (2003). Peridotite from the pro-pilot Hole (PP1) of the Chinese continental scientific drilling project and its bearing on depleted and metasomatic upper mantle. *Acta Geologica Sinica* **77**, 492–509 (in Chinese).

Li, Z. A. (1995). The evolution characters of mantle heat flow beneath Songliao basin. *Geotectonica et Metallogenia* **19**, 108–112 (in Chinese).

Liou, J. G., Zhang, R. Y., Wang, X., Eide, E. A., Ernst, W. G. & Maruyama, S. (1996). Metamorphism and tectonics of high-*P* and ultrahigh-*P* belts in the Dabie–Sulu region, eastern central China. In: Yin, A. & Harrison, T. M. (eds) *The Tectonics of Asia*. New York: Cambridge University Press, pp. 303–334.

Liou, J. G., Hacker, B. R. & Zhang, R. Y. (2000). Into the forbidden zone. *Science* **287**, 1215–1216.

Liu, D. Y., Nutman, A. P., Compston, W., Wu, J. S. & Shen, Q. H. (1992). Remnants of 3800 Ma crust in Chinese part of the Sino-Korean craton. *Geology* **20**, 339–342.

Liu, F. L., Xu, Z. Q., Katayama, I., Yang, J. S., Maruyama, S. & Liou, J. G. (2001). Mineral inclusions in zircons of para- and orthogneiss from pre-pilot drillhole CCSD-PP1, Chinese Continental Scientific Drilling Project. *Lithos* **59**, 199–215.

Lu, F. X. & Zheng, J. P. (1996). Paleozoic nature and deep processes of lithospheric mantle beneath North China. In: Chi, J. S. & Lu, F. X. (eds) *Kimberlites and Paleozoic Mantle beneath North China platform*. Beijing: Science Press (in Chinese).

Lu, F. X., Wang, Y., Chen, M. H. & Zheng, J. P. (1998). Geochemical characteristics and emplacement ages of the Mengyin kimberlites, Shandong Province, China. *International Geology Review* **40**, 998–1006.

Lu, F. X., Zheng, J. P., Li, W. P., Chen, M. H. & Chen, Z. M. (2000). The mantle evolution pattern of Phanerozoic mantle in the eastern China: the 'Mushroom Cloud' model. *Geoscience Frontier* **7**, 97–107 (in Chinese).

Lu, F. X., Wang, C. Y., Zheng, J. P. & Zhang, R. S. (2003). Lithospheric composition and structure of north boundary of Qinling: study on deep-seated xenoliths from Minggang area of Henan Province. *Science in China (Ser. D)* **33**, 1–9 (in Chinese).

Downloaded from http://petrology.oxfordjournals.org/ at University of New Orleans on June 26, 2014

Ma, X., Liu, G. & Su, J. (1984). The structure and dynamics of the continental lithosphere in north-northeast China. *Annual Geophysics* **1**, 611–620.

McDonough, W. F. & Sun, S. S. (1995). The composition of the Earth. *Chemical Geology* **120**, 223–253.

Medaris, L. G. (1999). Garnet peridotite in Eurasian HP and UHP terranes: a diversity of origins and thermal histories. *International Geology Review* **41**, 799–815.

Meen, J. K. (1987). *Mantle Metasomatism and Carbonates: an Experimental Study of a Complex Relationship. Geological Society of America, Special Papers* **215**, 91–100.

Menzies, M. A. & Xu, Y. G. (1998). Geodynamics of the North China Craton. In: Flower, M., Chung, S. L. & Lo, C. H. (eds) *Mantle Dynamics and Plate Interactions in East Asia. American Geophysical Union, Geodynamics Series,* **27**, 155–165.

Menzies, M. A., Fan, W. M. & Zhang, M. (1993). Paleozoic and Cenozoic lithoprobes and loss of >120 km of Archean lithosphere, Sino-Korean craton, China. In: Prichard, H. M., Alabaster, T., Harris, N. B. W. & Neary, C. R. (eds) *Magmatic Processes and Plate Tectonics. Geological Society, London, Special Publications* **76**, 71–81.

Okay, A. I., Xu, S. & Sengor, A. M. C. (1989). Coesite from the Dabie Mountains eclogite, central China. *European Journal of Mineralogy* **1**, 595–598.

O'Neill, H. St. C. & Wood, B. J. (1979). An experimental study of Fe–Mg partitioning between garnet and olivine and its calibration as a geothermometer. *Contributions to Mineralogy and Petrology* **70**, 59–70.

O'Reilly, S. Y. & Griffin, W. L. (1985). A xenolith-derived geotherm for southeastern Australia and its geophysical implications. *Tectonophysics* **111**, 41–63.

O'Reilly, S. Y., Chen, D., Griffin, W. L. & Ryan, C. G. (1996). Minor elements in olivine from spinel lherzolite xenoliths: implications for thermobarometry. *Mineralogy Magazine* **61**, 257–269.

O'Reilly, S. Y., Griffin, W. L., Poudjom Djomani, Y. & Morgan, P. (2001). Are lithospheres forever? Tracking changes in subcontinental lithspheric mantle through time *GSA Today* **11**, 4–9.

Pouchou, J. L. & Pichoir, F. (1984). A new model for quantitative X-ray microanalysis. Part 1: application to the analysis of homogeneous samples. *Recherche Aerospatiale* **5**, 13–38.

Poudjom Djomani, Y. H., O'Reilly, S. Y., Griffin, W. L. & Morgan, P. (2001). The density structure of subcontinental lithosphere: constraints on delamination models. *Earth and Planetary Science Letters* **184**, 605–621.

Rudnick, R. L., Gao, S., Ling, W. L., Liu, Y. S. & McDonough, W. F. (2004). Petrology and geochemistry of spinel peridotite xenoliths from Hannuoba and Qixia, North China craton. *Lithos* **77**, 609–637.

Ryan, C. G., Griffin, W. L. & Pearson, N. L. (1996). Garnet geotherms: pressure–temperature data from Cr-pyrope garnet xenocrysts in volcanic rocks. *Journal of Geophysical Research* **101**, 5611–5625.

Schreyer, W. (1988). Experimental studies on metamorphism of crustal rocks under mantle pressure. *Mineralogy Magazine* **52**, 1–26.

Stalder, R., Foley, S. F., Brey, G. P. & Horn, I. (1998). Mineral–aqueous fluid partitioning of trace elements at 900–1200°C and 3·0–5·7 GPa: new experimental data for garnet, clinopyroxene, and rutile, and implications for mantle metasomatism. *Geochimica et Cosmochimica Acta* **62**, 1781–1801.

Sun, J. Y. (1992). A seismic tomography profile cross the Sino-Korean craton. *Information of Geoscience and Geotechnique* **11**, 4–13 (in Chinese).

van Achterbergh, E., Ryan, C., Jackson, S. & Griffin, W. L. (2001). Data reduction software for LA-ICP-MS. In: Sylvester P. (ed.) *Laser-Ablation–ICPMS in the Earth Sciences. Mineralogical Association of Canada, Short Courses* **29**, 239–243.

Wang, X. M., Liou, J. G. & Mao, H. K. (1989). Coesite-bearing eclogites from the Dabie Mountains in central China. *Geology* **17**, 1085–1088.

Xu, S. T., Okay, A. I., Ji, S., Sengor, A. M. C., Kiu, Y. & Jiang, L. (1992). Diamond from the Dabie Shan metamorphic rocks and its implication for tectonic setting. *Science* **256**, 80–92.

Xu, X., O'Reilly, S. Y., Griffin, W. L. & Zhou, X. (1998). The nature of the Cenozoic lithosphere at Nushan, eastern China. In: Flower, M., Chung, S. L. & Lo, C. H. (eds) *Mantle Dynamics and Plate Interactions in East Asia. American Geophysical Union, Geodynamics Series* **27**, 167–196.

Xu, X., O'Reilly, S. Y., Griffin, W. L. & Zhou, X. (2000). Genesis of young lithospheric mantle in southeastern China: a LAM–ICPMS trace element study. *Journal of Petrology* **40**, 111–148.

Xu, Y. G. (2001). Thermo-tectonic destruction of the Archean lithospheric keel beneath the Sino-Korean craton in China: evidence, timing and mechanism. *Physics and Chemistry of the Earth (A)* **26**, 747–757.

Xu, Y. G., Lin, C. Y., Shi, L. B., Mercier, J. C. C. & Ross, J. V. (1995). Upper mantle geotherm for eastern China and its geological implications. *Science in China (Series B)* **38**, 1482–1492.

Yang, J. J. & Jahn, B. M. (2000). Deep subduction of mantle-derived garnet peridotites from the Su-Lu UHP metamorphic terrane in China. *Journal of Metamorphic Geology* **18**, 167–180.

Yang, J. J., Godard, G., Kienast, J. R., Lu, Y. & Sun, J. (1993). Ultrahigh-pressure (60 kbar) magnesite-bearing garnet peridotites from northeastern Jiangsu, China. *Journal of Geology* **101**, 541–554.

Yaxley, G. M., Crawford, A. J. & Green, G. H. (1991). Evidence for carbonatite metasomatism in spinel peridotite xenoliths from western Victoria, Australia. *Earth and Planetary Science Letters* **107**, 305–317.

Yaxley, G. M., Green, D. H. & Kamenetsky, V. (1998). Carbonatite metasomatism in the southeastern Australia lithosphere. *Journal of Petrology* **39**, 1917–1930.

Ye, K., Cong, B. L. & Ye, D. N. (2000). The possible subduction of continental materials to depths greater than 200 km. *Nature* **407**, 334–336.

Yu, C. M., Zheng, J. P. & Griffin, W. L. (2006). LAM–ICPMS analysis on clinopyroxene of peridotite xenoliths from Hannuoba and its significance on lithospheric mantle evolution. *Earth Science* **31**, 93–100 (in Chinese).

Yuan, X. C. (1996). *Atlas of Geophysics in China*. Beijing: Geological Publishing House, 217 pp.

Zangana, N. A., Downes, H., Thirlwall, M. F., Marriner, G. F. & Bea, F. (1999). Geochemical variation in peridotite xenoliths and their constituent clinopyroxenes from Ray Pic (French Massif Central): implications for the composition of the shallow lithospheric mantle. *Chemical Geology* **153**, 11–35.

Zhai, M. G., Guo, J. H. & Liu, W. J. (2001). An exposed cross-section of early Precambrian continental lower crust in North China craton. *Physics and Chemistry of the Earth (A)* **26**, 781–792.

Zhang, A. D., Xu, D. H. & Xie, X. L. (1994). The status and future of diamond exploration in China. In: Meyer, H. O. & Leonardos, O. H. (eds) *Diamonds: Characterization, Genesis and Exploration. Proceedings of the Fifth International Kimberlite Conference, Araxa, Brazil. CPRM Special Publications* **IB**, 268–284.

Zhang, H. F., Sun, M., Zhou, X. H., Fan, W. M., Zhai, M. G. & Yin, J. F. (2002). Mesozoic lithosphere destruction beneath the North China Craton: evidence from major-, trace–element and Sr–Nd–Pb isotope studies of Fangcheng basalts. *Contributions to Mineralogy and Petrology* **144**, 241–253.

Zhang, H. F., Sun, M., Zhou, X. H., Zhou, M. F., Fan, W. M. & Zheng, J. P. (2003). Secular evolution of the lithosphere beneath

Downloaded from http://petrology.oxfordjournals.org/ at University of New Orleans on June 26, 2014

the eastern North China Craton: evidence from Mesozoic basalts and high-Mg andesites. *Geochimica et Cosmochimica Acta* **15**, 4373–4387.

Zhang, R. Y., Hirajima, T., Banno, S., Cong, B. L. & Liou, J. G. (1995). Petrology of ultrahigh pressure rocks from the southern Sulu region, eastern China. *Journal of Metamorphic Geology* **13**, 659–675.

Zhang, R. Y., Liou, J. G., Yang, J. S. & Yui, T. F. (2000). Petrochemical constrains for dual origin of garnet peridotites from the Dabie–Sulu UHP terrane, eastern–central China. *Journal of Metamorphic Geology* **18**, 149–166.

Zhang, R. Y., Liou, J. G., Yang, J. S. & Ye, K. (2003). Ultrahigh-pressure metamorphism in the forbidden zone: the Xugou garnet peridotite, Sulu terrane, eastern China. *Journal of Metamorphic Geology* **21**, 539–550.

Zhao, G. C., Wilde, S. A., Cawood, P. A. & Lu, L. Z. (1999). Thermal evolution of two textural types of mafic granulites in the North China craton: evidence for both mantle plume and collisional tectonics. *Geological Magazine* **136**, 223–240.

Zhao, G. C., Cawood, P. A., Wilde, S. A., Sun, M. & Lu, L. Z. (2000). Metamorphism of basement rocks in the Central Zone of the North China Craton: implications for Paleoproterozoic tectonic evolution. *Precambrian Research* **103**, 55–88.

Zheng, J. P. (1999). *Mesozoic–Cenozoic Mantle Replacement and Lithospheric Thinning, East China*. Wuhan: China University of Geosciences Press, 126 pp. (in Chinese).

Zheng, J. P. & Lu, F. X. (1999). Mantle xenoliths from kimberlites, Shandong and Liaoning: Paleozoic lithospheric mantle character and its heterogeneity. *Acta Petrologica Sinica* **15**, 65–74 (in Chinese).

Zheng, J. P., O'Reilly, S. Y., Griffin, W. L., Lu, F. X. & Zhang, M. (1998). Nature and evolution of Cenozoic lithospheric mantle beneath Shandong Peninsula, Sino-Korean craton. *International Geology Review* **40**, 471–499.

Zheng, J. P., O'Reilly, S. Y., Griffin, W. L., Lu, F. X., Zhang, M. & Pearson, N. J. (2001). Relics of refractory mantle beneath the eastern North China block: significance for lithosphere evolution. *Lithos* **57**, 43–66.

Zheng, J. P., Griffin, W. L., O'Reilly, S. Y., Lu, F. X., Wang, C. Y., Zhang, M., Wang, F. Z. & Li, H. M. (2004a). 3·6 Ga lower crust in central China: new evidence on the assembly of the North China Craton. *Geology* **32**, 229–232.

Zheng, J. P., Griffin, W. L., O'Reilly, S. Y., Lu, F. X. & Yu, C. M. (2004b). U–Pb and Hf-isotope analysis of zircons in mafic xenoliths from Fuxian kimberlites: evolution of the lower crust beneath the North China Craton. *Contributions to Mineralogy and Petrology* **148**, 79–103.

Zheng, J. P., Zhang, R. Y., Liou, J. G., Griffin, G. L. & O'Reilly, S. Y. (2005a). A heterogeneous and metasomatic mantle recorded by trace elements of minerals from Donghai garnet peridotite in the Sulu UHP terrane, China. *Chemical Geology* **221**, 243–259.

Zheng, J. P., Sun, M., Zhou, M. F. & Robinson, P. (2005b). Trace elemental and PGE geochemical constraints of Mesozoic and Cenozoic peridotitic xenoliths on lithospheric evolution of the North China Craton. *Geochimica et Cosmochimica Acta* **69**, 3401–3418.

Zheng, J. P., Griffin, W. L., O'Reilly, S. Y., Liou, J. G., Zhang, R. Y. & Lu, F. X. (2005c). Late Mesozoic–Eocene mantle replacement beneath the eastern North China Craton: evidences from the Paleozoic and Cenozoic peridotite xenoliths. *International Geology Review* **47**, 457–472.

Zheng, J. P., Griffin, W. L., Zhang, H. F., Yu, C. M., O'Reilly, S. Y. & Zhang, M. (2006a). Peridotite xenoliths from late Mesozoic (∼100 Ma) Fuxin basalts: Significance for the mechanism and starting time of lithosphereic thinning with mantle replacement beneath the eastern North China Craton. *Lithos* (in review).

Zheng, J. P., Griffin, W. L., O'Reilly, S. Y., Yang, J. S. & Zhang, R. Y. (2006b). A refractory mantle protolith in younger continental crust, east–central China: age and composition of zircon in the Sulu UHP peridotite. *Geology* **34**, 705–708.

Zhi, X. C., Chen, D. G. & Chen, Y. (1994). The neodymium and strontium isotopic compositions of Cenozoic alkalic basalts from Penglai and Lingqu, Shandong Province. *Geological Review* **40**, 526–533 (in Chinese).

Zhou, J., Griffin, W. L., Jaques, A. L., Ryan, C. G. & Win, T. T. (1994). Geochemistry of diamond indicator minerals from China. In: Meyer, H. O. A. & Leonardos, O. H. (eds) *Diamonds: Characterization, Genesis and Exploration. CPRM Special Publications* **1B/93**, 285–301.

Downloaded from http://petrology.oxfordjournals.org/ at University of New Orleans on June 26, 2014